applied sciences

MDPI

Review

The Development Progress of Surface Structure Diffraction Gratings: From Manufacturing Technology to Spectroscopic Applications

Ye Wang [1,2], Xiuhua Fu [1,*], Yongyi Chen [2,3,*], Li Qin [2], Yongqiang Ning [2] and Lijun Wang [2,4,5,*]

1 School of Opto-Electronic Engineering, Changchun University of Science and Technology, Changchun 130022, China; wyoptics@163.com
2 Changchun Institute of Optics, Fine Mechanics and Physics, Chinese Academy of Sciences, Changchun 130033, China; qinl@ciomp.ac.cn (L.Q.); ningyq@ciomp.ac.cn (Y.N.)
3 Jlight Semiconductor Technology Co., Ltd., No. 1783, Zibo Road, ETDZ, Changchun 130102, China
4 Peng Cheng Laboratory, No. 2, Xingke 1st Street, Shenzhen 518000, China
5 Academician Team Innovation Center of Hainan Province, Key Laboratory of Laser Technology and Optoelectronic Functional Materials of Hainan Province, School of Physics and Electronic Engineering, Hainan Normal University, Haikou 570206, China
* Correspondence: goptics@126.com (X.F.); chenyy@ciomp.ac.cn (Y.C.); wanglj@ciomp.ac.cn (L.W.); Tel.: +86-136-0440-5770 (X.F.); +86-180-4304-7205 (Y.C.); +86-135-0088-0855 (L.W.)

Abstract: The high-precision diffraction grating is an important chromatic dispersion component that has been widely used in many fields, including laser beam combining, chirped pulse compression, spectroscopy, among others. In this paper, we review the development status of reflection and transmission gratings with high diffraction efficiency and high laser-induced damage thresholds, such as metal-film and multilayer-dielectric-film gratings. Then, we review the basic principles and most recent stages in the development of manufacturing techniques, such as mechanical scribing, holographic exposure, electron-beam lithography, and nanoimprinting.

Keywords: metal-film grating; multilayer-dielectric-film grating; grating preparation technology; diffraction efficiency; laser-induced damage threshold; diffraction grating

Citation: Wang, Y.; Fu, X.; Chen, Y.; Qin, L.; Ning, Y.; Wang, L. The Development Progress of Surface Structure Diffraction Gratings: From Manufacturing Technology to Spectroscopic Applications. *Appl. Sci.* **2022**, *12*, 6503. https://doi.org/10.3390/app12136503

Academic Editor: Edik U. Rafailov

Received: 8 June 2022
Accepted: 24 June 2022
Published: 27 June 2022

1. Introduction

Diffraction gratings are diffractive optical elements with periodic structures that divide light comprised of different wavelengths into spectra. These spectra may be used to investigate the structure or composition of experimental materials. With the rapid advancement of science, there is an exceptionally high demand in the optical industry for highly integrated micro-nano optoelectronic devices. Micro-nano-structured diffraction grating devices with periodic variation and diffraction capabilities simultaneously offer superior integration, accuracy, and efficiency. Diffraction gratings are widely used in many fields, including laser beam combining [1–3], chirped pulse compression [4–6], spectroscopy [7–9], and liquid crystal displays and photonic devices [10]. Gratings can be classified as transmission or reflection gratings based on the material used; however, the principles of functioning can vary widely among gratings of the same type. A thin grating, for example, is defined as a grating that generates Raman-Nas state diffraction and may alternatively be defined as a grating with a narrow angle and wavelength selectivity. Thick gratings (or volume gratings) are gratings that cause Bragg zone diffraction. In contrast to the diffraction state formulation, there is a straightforward boundary ($d/\Lambda = 10$) between thin and thick grating diffraction. This term has been thoroughly researched in several papers [11]. Diffraction gratings come in a variety of shapes and sizes, such as thin gratings, with new design methodologies introduced to achieve extremely high efficiency and volume gratings with new structures and materials, inter alia [12–14]. In this paper, our

study focuses on metal-film and multilayer-dielectric-film gratings to achieve extremely high diffraction efficiency and high laser-induced damage thresholds.

As early as the 1780s [15], the American astronomer D. Rittenhouse fabricated a transmission grating with a width of 12.7 mm using thin wires and saw a blurred color image through a shutter in a dark room, which was the first chromatic dispersion experiment using a grating. J. von Fraunhofer fabricated a 315 lines/mm reflection grating in 1823 by carving grooves on a glass surface covered with gold film. He established grating theory by first measuring the wavelengths of light and explaining the phenomena of diffraction and then deriving the grating equation. In 1870, L. M. Rutherford produced a diffraction grating with a line density of 860 lines/mm, the resolution of which surpassed that of a prism for the first time, which made a great stride in spectral analysis technology into a new century. H. A. Rowland, regarded as the inventor of modern diffraction gratings, used the mechanical scribing method. However, the production cycle of this method is extensive, and requires high experimental condition standards, which present substantial challenges in grating manufacture. After the passage of time and the continuous in-depth research of scientists, J. M. Burch in the United Kingdom fabricated gratings through holography for the first time in the 1950s. D. Rudolph et al. in Germany demonstrated the feasibility of producing gratings through holography in the late 1960s. Since then, grating manufacturing has advanced to a new level, with the development of key novel methods, such as holographic lithography, electron-beam lithography, and nanoimprinting.

The production of diffractive optical elements and their use in spectroscopy contribute significantly to scientific, economic, and social development. This review outlines the current state of diffraction grating development. Metal gratings, dielectric-film gratings, and significant technical indicators are examined in the first part. The second part describes grating preparation techniques, including mechanical scribing, holographic exposure, electron-beam lithography, and nanoimprinting. The third part provides a summary and considers future prospects for diffraction gratings.

2. High Diffraction Efficiency and Damage-Resistance Threshold Gratings

Diffraction efficiency is an essential technical indicator for evaluating the performance of a diffraction grating. In actual research, it is necessary to meet certain parameter requirements. For example, optimizing the grating groove type and duty cycle, along with other parameters, is required to obtain a diffraction grating with a high diffraction efficiency and anti-laser-damage threshold. An overview of metal-film reflection, multilayer-dielectric-film reflection, and multilayer-dielectric-film transmission gratings is provided below.

2.1. Metal-Film Reflection Gratings

American researchers developed the first diffraction gratings using metal wires in the 18th century. The surface of a typical reflection grating with a high diffraction efficiency is gold-plated, making use of the strong metal conductivity to achieve high reflectivity and increased reflection and diffraction efficiencies. I. Yamada et al. [16] created a single-layer tungsten–silicide-metal grating using double-beam interference lithography and dry etching in 2008. The period of this grating was 400 nm, the groove depth was 350 nm, and the duty cycle was 0.6. Above 5 m, the transverse magnetic (TM) transmission exceeded 50%, and the estimated extinction ratio was approximately 20 dB. Figure 1 provides a scanning electron microscope (SEM) image of the infrared metal-grating surface morphology, along with the polarization characteristics.

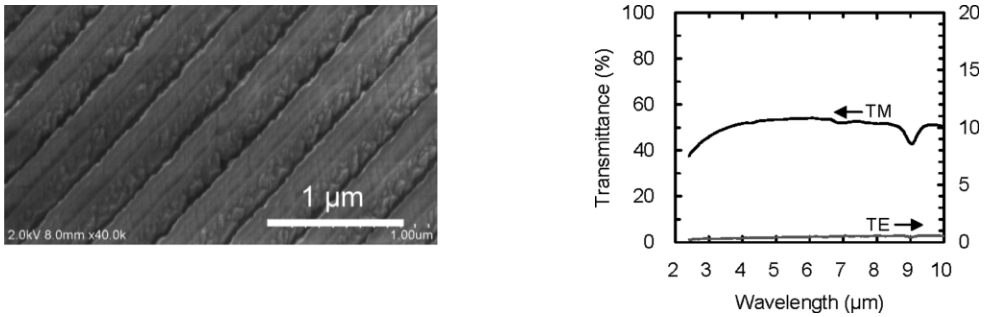

Figure 1. Surface topography SEM image of the infrared grating (groove depth = 350 nm, period (Λ) = 400 nm, and duty cycle (f) = 0.6) and its polarization characteristics.

In 2010, S. Peng, L. Quan, and W. Jianhong [17] created a subwavelength metal polarization grating for polarization imaging in the visible-light range. Figure 2 depicts a schematic diagram of the grating construction. Finite-difference time-domain (FDTD) simulation was used to determine the ideal grating parameters: the period was 200 nm, the aluminum thickness was 260 nm, and the duty cycle was 0.4. The transmission efficiency in the visible-light band was higher than 50%, with a maximum value of 70%. The extinction ratio was greater than 3.5×10^3, with a maximum value of approximately 5.5×10^4.

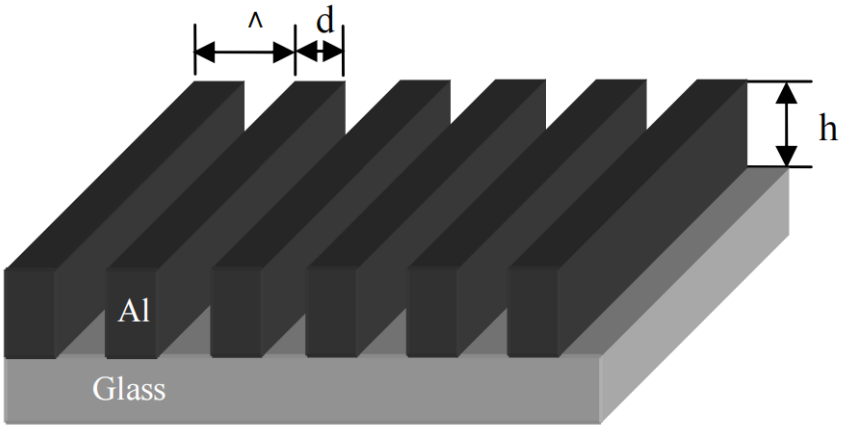

Figure 2. Structural model of subwavelength metal polarization grating.

In 2012, Q. Jin, Q. Liu, et al. [18] used a two-beam interference lithography procedure combined with a reactive-ion etching approach and a nanoimprinting process to produce a single-layer aluminum-metal grating on a chalcogenide–glass substrate. The metal grating had a period of 500 nm and a height of 130 nm. The structure comprising a 120 nm Al layer and a 50 nm anti-reflection Cu layer was established with resist-substrate reflectivity and the ultimate performance of the polarizer in mind. The TM transmission efficiency was greater than 71%, and the extinction ratio was greater than 25 dB. The TM transmission was greater than 60% in the 5–9 m range, and the extinction ratio was greater than 20 dB in the 2.5–11 m range. N. Jing et al. [19] at Wuhan Huake University proposed a metal grating with a sandwiched Au-Si-Au structure in 2014 and obtained a TM transmission performance greater than 90% through simulation calculations.

Z. Xia, H. Huang, et al. [20] researched and fabricated gold-coated gratings for pulse compression in 2017. The grating structural parameters were: period 574.7 nm, duty cycle 0.82, groove depth 232 nm, and a diffraction efficiency greater than 90% in the 700–1000 nm range. A Ti–sapphire laser system was used for a one-on-one laser-damage experiment on the diffraction grating. Figure 3 illustrates the damage morphology and laser energy density measured at 60 fs under 0.95 J/cm^2.

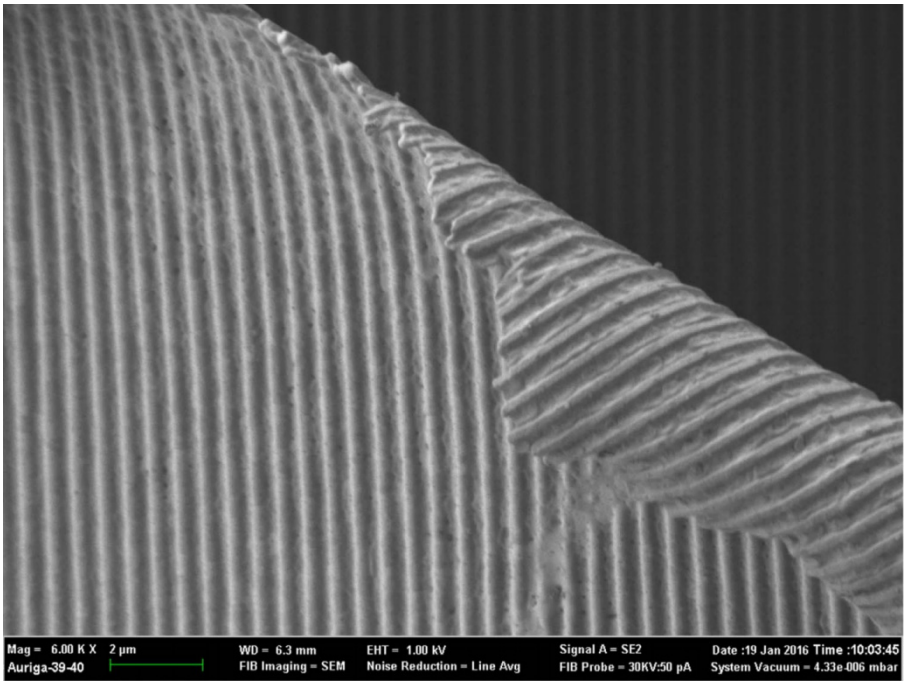

Figure 3. Laser-induced damage morphology of gold-coated grating. The basic grating material was photoresist, and the surface gold film was deposited by the electron-beam evaporation method. The laser energy density was 0.95 J/cm^2, the wavelength was 800 nm, and the pulse width was 60 fs. The laser was incident at the top-left side. A one-on-one test mode was used in the experiment.

Z. Xia, Y. Wu, et al. [21] designed a gold-coated grating in 2018. The period of the grating was 574.7 nm, the groove depth was 232 nm, the duty cycle was 0.82, and the −1 order of the grating was constructed in the 700–1000 nm band. The diffraction efficiency was greater than 90%. For damage investigations, a CPA Ti–sapphire laser system was implemented, and the laser-damage threshold of the manufactured grating was 0.62 J/cm^2. As shown in Figure 4.

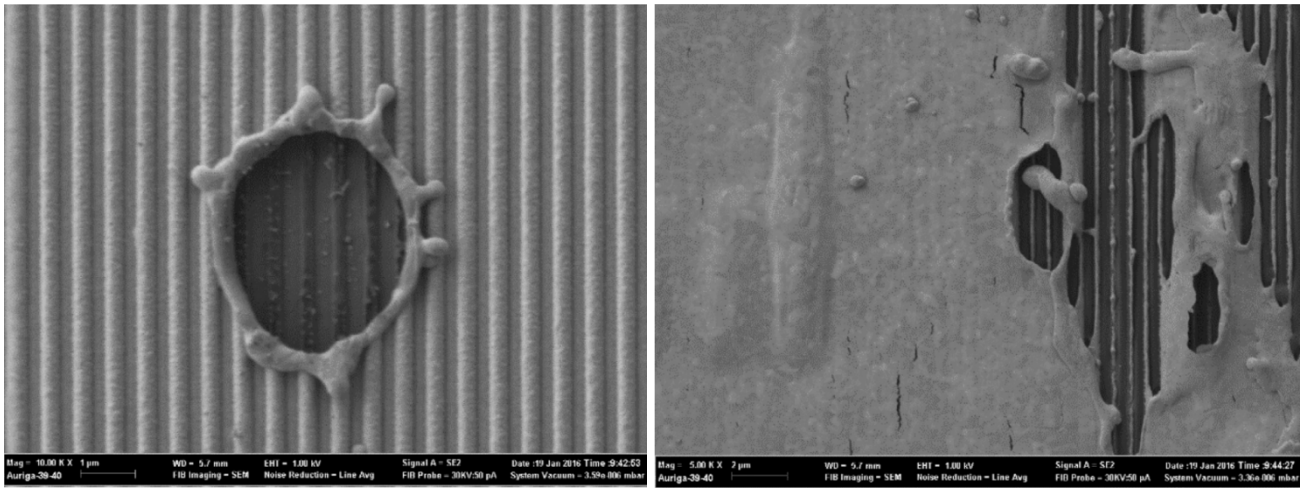

Figure 4. Damage morphology of the gold-coated grating.

Due to their absorption properties, metal gratings have low anti-laser-damage thresholds and diffraction efficiencies [22]. There have been few reports in recent years on the production and application of metal gratings. A summary of the above analysis is shown in Table 1. No photoresist coating is utilized in the grating construction to optimize and improve the performance of the metal grating. The substrate may be immediately scribed,

and then a metal film and a protective layer can be coated on it, considerably improving the metal grating's diffraction efficiency and laser-damage resistance. To successfully overcome the aforementioned challenges, an increasing number of researchers have concentrated on film gratings, resulting in a significant amount of attention and active study.

Table 1. Overview of metal film reflection gratings in recent years.

Years	Units	Structures	Performance
2008	Itsunari Yamada, et al. [16]	Period 400 nm, groove depth 350 nm, duty cycle 0.6	Transmittance TM > 50% (>5 μm), extinction ratio ≈ 20 dB
2010	Sun Peng, Liu Quan, et al. [17]	Period 200 nm, aluminum 260 nm, duty cycle 0.4	Transmission efficiency > 45%, extinction ratio > 3.5×10^3
2012	Qiufeng Jin, Quan Liu, et al. [18]	Period 500 nm, ridge height 130 nm, Al 120 nm, Cu 50 nm	Transmittance TM > 60% (5–9 μm), extinction ratio ≈ 20 dB (2.5–11 μm)
2014	Jing Nie, et al. [19]	Au-Si-Au	Transmission TM > 90%
2017	Zhilin Xia, Haopeng Huang, et al. [20]	Period 574.7 nm, duty cycle 0.82, groove depth 232 nm	DE > 90% @700–1000 nm, LIDT = 0.95 J/cm^2 @60 fs
2018	Yihan Wu, Zhilin Xia, et al. [21]	Period 574.7 nm, groove depth 232 nm, duty cycle 0.82	−1st DE > 90% @700–1000 nm, LIDT = 0.62 J/cm^2

2.2. Multilayer-Dielectric-Film Grating

Gabor pioneered the concept of holographic optics in the 20th century. With the advancement and maturation of laser technology, the technology of preparing gratings under laser interference conditions (holographic exposure), has been developed. This technology can produce large-area diffraction gratings with good uniformities and diffraction efficiencies, which has promoted the rapid development of grating theory. The limitations in metal-grating performance have driven scientific researchers to constantly innovate to meet more stringent requirements, and multilayer-dielectric-film gratings have been developed one after the other. Dielectric-film gratings are feasible because the inherent absorbance of dielectric materials is approximately zero. The diffraction efficiency is 100%, and the damage-resistance thresholds are many orders of magnitude higher than those of metal gratings. The grating period, duty cycle, groove depth, and residual thickness of the top relief structure without etching are the most important structural characteristics of multilayer-dielectric-film gratings. The diffraction effectiveness of a multilayer-dielectric-film grating is affected by the incident angle and wavelength of the incoming light, as well as the groove depth, duty cycle, groove structure, multilayer-dielectric-film structural parameters, and surface relief-structure refractive index. To develop a diffraction grating with a high diffraction efficiency and anti-laser-damage threshold, it is necessary to use software to optimize the design of the film-stack structure of the multilayer bonding film and structural parameters of the diffraction grating. This design process results in a multilayer-dielectric-film grating with good performance. The development process of the topmost multilayer dielectric film is to continually improve the diffraction efficiency and anti-laser-damage threshold, as well as the preparation procedure [23–26].

2.2.1. Multilayer-Dielectric-Film Reflection Grating

The concept of multilayer-dielectric-film gratings was initially presented by the Lawrence Livermore National Laboratory (LLNL) in the United States in 1992. A diffraction efficiency greater than 98% can be achieved by adjusting the characteristics of the groove structure. For the first time, in 1993, the LLNL constructed the multilayer dielectric grating created the previous year. At 1053 nm, the incident wavelength had the maximum diffraction effectiveness. The grating was made up of eight pairs of dielectric-film materials with high and low refractive indices. The periodic relief structure was transmitted

to the dielectric layer, and the as-prepared grating diffraction effectiveness was greater than 97% [27,28].

D. Perry, R. D. Boyd, et al. [29] created a novel high-efficiency multilayer-dielectric-film reflection grating in California in 1995. The reflection and diffraction efficiency of first-order polarized light is greater than 96% due to the correct design of the multilayer dielectric film stack structure and grating structure, and the simulated theoretical diffraction efficiency is given in Figure 5. The scribe line density was 1550 gr/mm, the incident wavelength was 1053 nm, and the Littrow angle in transverse electric (TE) mode was 56°. The multilayer dielectric film was made of ZnS and ThF_4, with ZnS serving as the top layer. Figure 6 depicts the prepared raster SEM image.

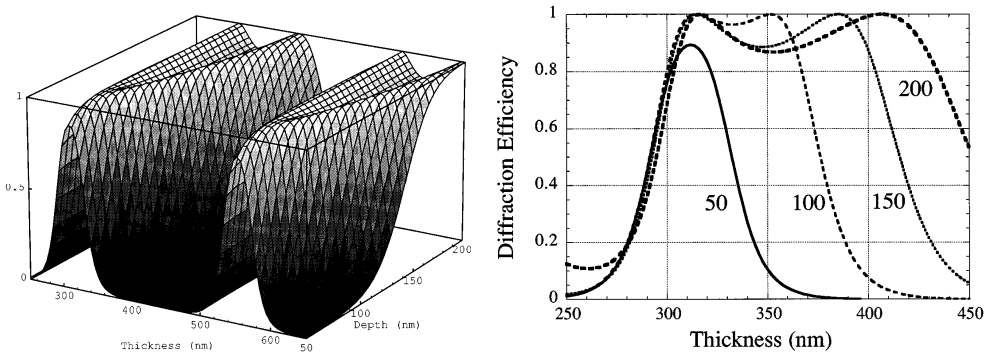

Figure 5. Theoretical diffraction efficiency.

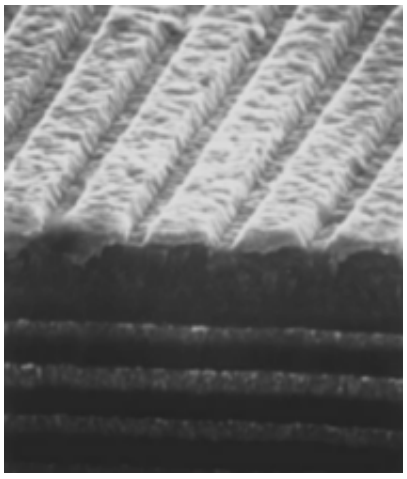

Figure 6. Cross-sectional SEM image of the 1550 gr/mm grating.

B. W. Shore, M. D. Perry, et al. [30] created an effective all-dielectric reflection grating in 1997. Figure 7 depicts the grating design structure. This multilayer-dielectric-film reflection grating was TE polarized, with a center wavelength of 1053 nm, line density of 1480 lines/mm, Littrow angle of 51.2°, duty cycle of 0.3, and first-order reflection and diffraction efficiency of 95%. The multilayer dielectric film structure is $(HLL)^n$ (H: HfO_2, and L: SiO_2). Figure 7a shows that the top-layer structure is a high-refractive-index material, with the highest or lowest diffraction efficiency, and Figure 7b shows that the top-layer groove is a high-refractive-index material. A large groove depth is required to achieve higher performance indicator values when the top structure is made of a low-refractive-index material. The groove depth in the 900 nm surface-layer thickness is 700 nm (200 nm subgroove thickness) (Figure 8), demonstrating the high-efficiency performance of the grating. This design example shows that H or L can be selected for the top structure to obtain a high-efficiency solution, but the etching material and the ability to resist the damage threshold must still be considered (higher with low-index material on the top layer).

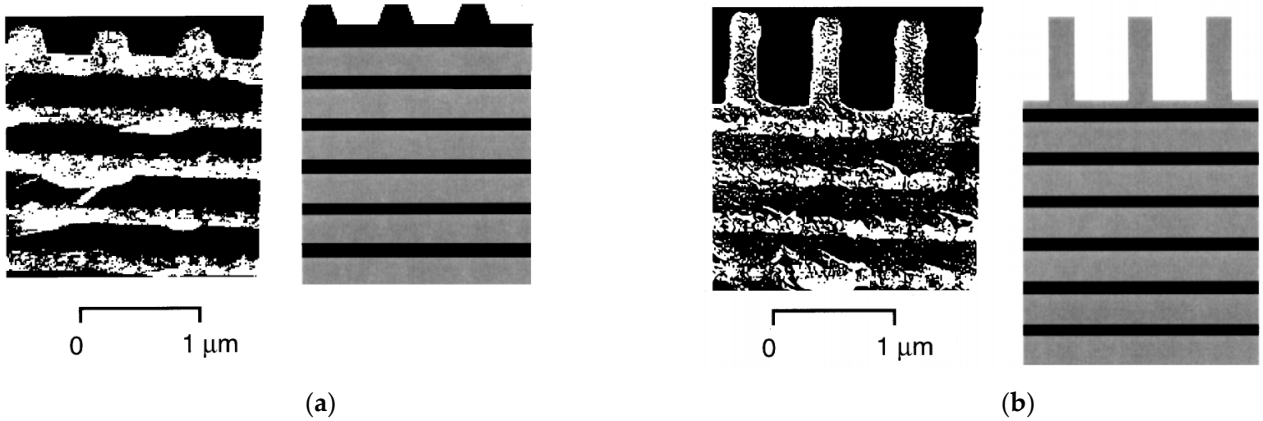

Figure 7. Multilayer dielectric designs of high-index (H) and low-index (L) layers, showing relative locations of substrate, multilayers, and groove corrugations (G). (**a**) Overcoated grating; dielectric layers effectively form a volume grating. (**b**) Undercoated grating; layers form a high-reflectivity (HR) stack under the corrugations.

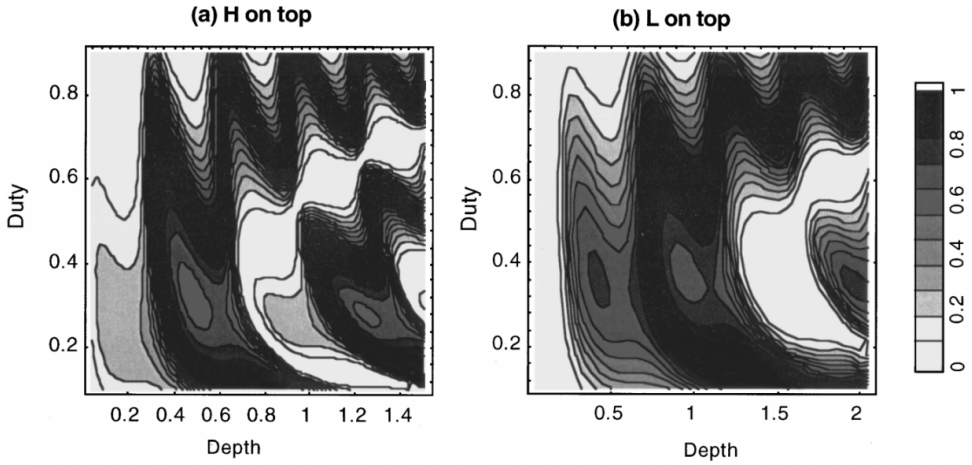

Figure 8. Efficiency versus depth and duty cycle for a quarter-wave HR stack, with grooves etched completely through the top layer. The grating grooves are lamellar, with 1480 grooves/mm, and the duty cycle is 0.3. The wavelength is 1053 nm at a Littrow angle of 51.2°, with TE polarization. The high-index material is hafnia, and the low-index material is silica. The quarter-waves are defined for the wavelength and angle used. (**a**) High-index surface layer over $(HL)^7$ stack. (**b**) Low-index surface layer over $(HL)^7$ H stack.

Intense laser light may readily destroy the gratings used in chirped pulse amplification (CPA) devices. To minimize damage and ensure that all incident laser light was reflected to just one diffraction order with a diffraction efficiency close to 100%, K. Hehl, J. Bischoff, et al. [31] presented a complete dielectric reflection grating in 1999, which was primarily formed from a multilayer-dielectric-reflective film and grating layer with a SiO_2 top structure. In this study, sputtering was used to deposit multilayer dielectric films. The multilayer film stack had the structure $(HL)^{10}L$, where H and L are Nb_2O_5 and SiO_2, respectively. The preparation accuracy and repeatability error were approximately 1%. Electron-beam lithography and ion-beam etching were used to create the grating structure with a period of 380 nm. Figure 9 is an SEM view of the as-constructed diffraction grating. In the Littrow structure, the incident wavelength was 532 nm and the angle of incidence was 45°, with TE polarization. The efficiency was 97% in first-order diffraction (3% loss owing to ghosting and scattering). The anti-laser-damage threshold of the dielectric grating measured by 5 ns laser pulse was 4.4 J/cm^2, and the anti-laser-damage threshold for a 1 ps laser pulse was 0.18 J/cm^2. These values are equivalent to those of a typical gold grating.

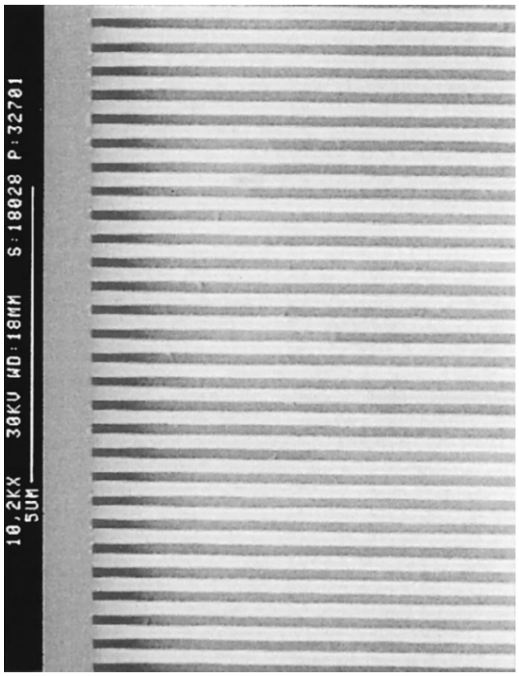

Figure 9. SEM image of the dielectric grating.

W. Hongbo and L. Lifeng conducted research in 2003 on the physical mechanism of achieving high efficiency in multilayer-dielectric-film reflection gratings with a −1 order Littrow structure, viewing the entire grating as a combination of two independent subsystems, the surface-relief grating and the multilayer-dielectric-film structure. Matrix equations help to understand the inherent physical mechanism of achieving high diffraction efficiency [32].

Destouches, A. V. Tishchenko, et al. [33] designed a resonant diffraction grating with a total dielectric reflection grating period of 560 nm, an incident wavelength of 1064 nm, and an incident angle of 73° in 2005, and a −1st order reflection diffraction efficiency of 99% under the non-Littrow structure. The high-efficiency diffraction grating proposed in this paper contrasts starkly with the previous gratings pioneered by Perry et al. It is simple to construct, and a groove structure with a depth of tens of nanometers may achieve high diffraction efficiency. As shown in Figure 10.

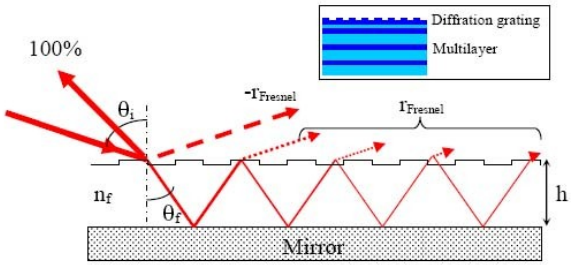

Figure 10. Fresnel reflection mechanism on a mirror-based corrugated dielectric film: direct reflection, field trapping, leaky-mode propagation, and re-radiation. The corrugation balances the direct-reflected and re-radiated field moduli, ensuring 100% −1st-order efficiency. The inset represents the fabricated multilayer-grating structure.

J. Neauport, E. Lavastre, et al. [34] investigated and constructed a multilayer-dielectric-reflection grating for ultrahigh-intensity laser-compressor applications in 2007. The density of the grating lines was 1780 lines/mm, and the incident angle was 70.6°. The dielectric film stack structure was $(HL)^7H$ (H and L are HfO_2 and SIO_2, respectively), with a reflectivity of 99.5% at 1053 nm. H. J. Yvon created the grating, and Figure 11 depicts the atomic force microscopy (AFM) test-groove profile. In order to investigate the anti-laser-damage

threshold, a one-to-one test was performed utilizing a laboratory-developed CPA laser system. Figure 12 depicts the findings for a 1740 lines/mm gold-plated grating tested under 72.5° TM polarization, which are similar to the previous results, with a high level of consistency [35–39]. The anti-laser-damage threshold of the multilayer-dielectric-reflecting grating disclosed in this study is 3.5–5 J/cm^2, which is substantially higher than the previously published multilayer-dielectric-grating data. The laser-induced damage threshold at 1 ps on a 77.2° and 1780 lines/mm multilayer dielectric grating was 2.5 J/cm^2, which was similar to the 2 J/cm^2 at 500 fs reported by Barty [36]. The laser-induced damage threshold of Keck's [37] 1740 lines/mm multilayer dielectric grating was 5.16 J/cm^2 at 10 ps, which is comparable to 2.6 J/cm^2 at 500 fs. E^2 determines the damage threshold.

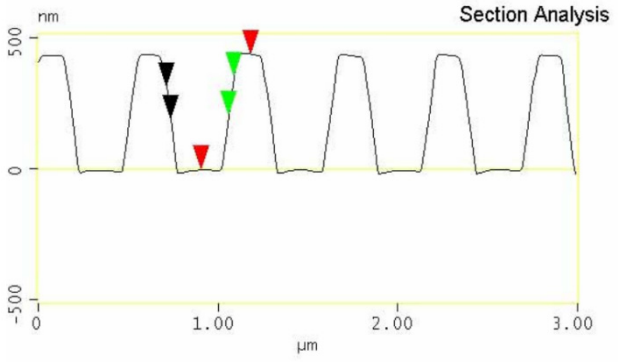

Figure 11. AFM measurement on a PW08 sample (section analysis).

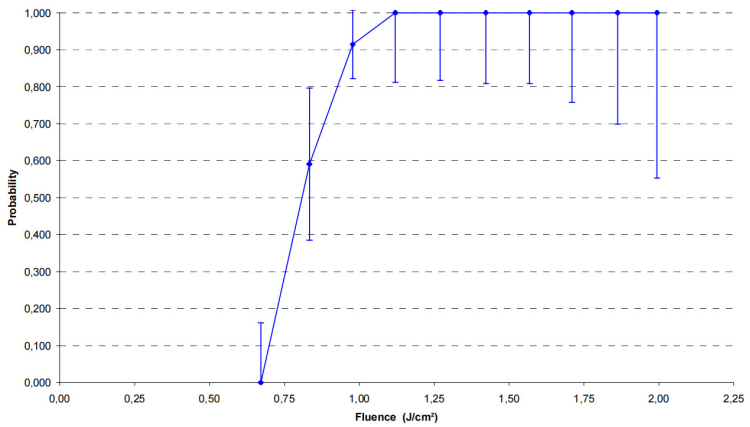

Figure 12. Example of damage probability on a 1740 lines/mm gold grating. Testing was performed at an incidence of 72.5° in TM polarization mode. The damage threshold (maximum value at which the damage probability is null) is 0.67 J/cm^2.

Wirth et al. [40] combined four 2.1 kW fiber lasers with a polarization-independent reflection grating to achieve an output power of up to 8.2 kW in 2011. The efficiency of light and −1st order diffraction were both better than 95%.

Ultrafast lasers often require a main oscillator power amplifier arrangement to achieve high peak power and energy. Owing to nonlinear effects, fiber-based laser amplifiers have evident peak power restrictions, and CPA technology is frequently employed to overcome this, using prisms or gratings, but the downside of this approach is that there is a significant loss of diffractive optical components. Its efficiency was rather low until recent advances, and the stated value of diffraction efficiency of reflection gratings is improving, generally in the region of 95 to 97%. M. Rumpel, M. Moeller, et al. [41] developed a high-efficiency reflecting broadband compression grating in 2014. Figure 13 depicts the grating-layer structure analyzed, which consisted of 29 levels of dielectric films, with each layer shown. The angle of incidence was 44°, and the physical thickness of the high or low refractive

index film recorded. Interference lithography and reactive-ion-beam etching were used to create the grating layer. The grating had a 1250 lines/mm structure and a duty cycle of 0.25. Figure 14 shows a photograph and an SEM image. The efficiency was 99.35%, the diffraction efficiency in the 1060 nm band was 99.7%, and the anti-laser-damage threshold was 2.95 J/cm^2, as shown in Figure 15.

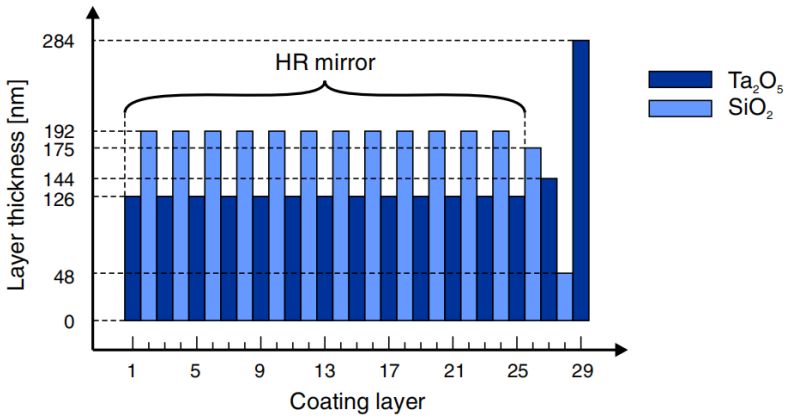

Figure 13. Schematic diagram of the reflection grating structure.

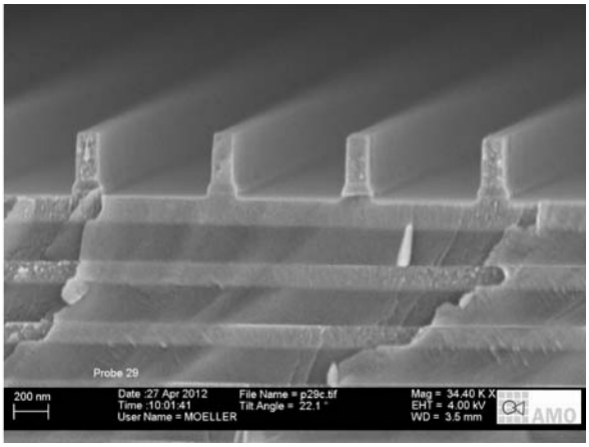

Figure 14. SEM image of the grating structure on a cleavage-test sample.

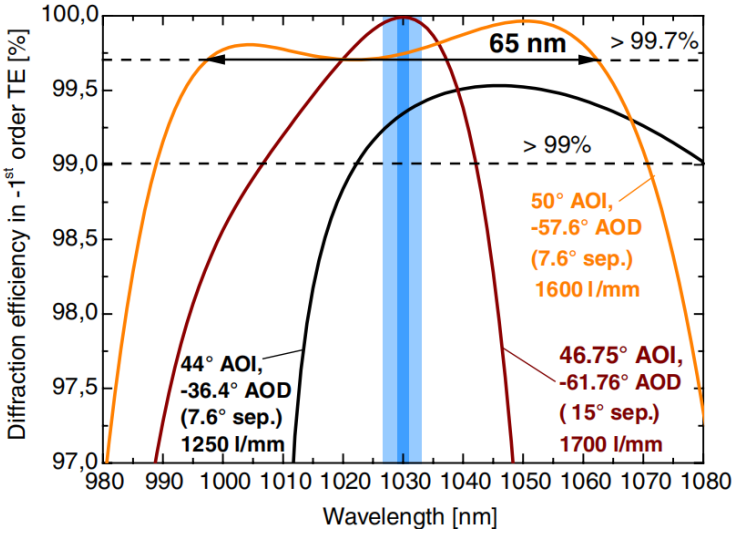

Figure 15. Relationship between the reflection grating and diffraction efficiency.

In 2016, Y. Zheng, Y. Yifeng, et al. [42] reported a spectral-beam-combining (SBC) system of eight 1.5 kW ytterbium-doped all-fiber superfluorescent light sources at a wavelength of 1070 nm, with the eight output elements coupled to a self-developed, polarization-independent, multilayer-dielectric-film reflection grating. The beam was spectrally mixed, with an output power of 10.8 kW and a combined efficiency of 94%. The grating line density was 960 lines/mm, and the diffraction efficiency in the 1040–1090 nm band at an incidence angle of 30.9° was greater than 95%, using the −1 order Littrow structure. As illustrated in Figure 16, M^2 = 1.9, the beam quality was adjusted by using the double-grating-dispersion correction system, and it was demonstrated that the double-grating configuration is a promising high-brightness SBC approach.

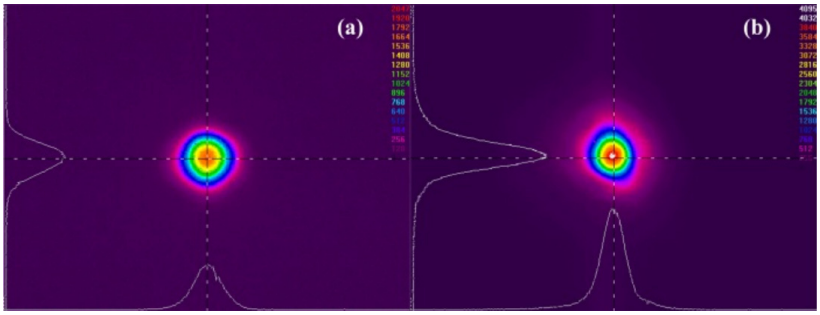

Figure 16. Far-field pattern of the combined beam in (**a**) a low-power case and (**b**) a full-power (3 kW) case in the dual-grating SBC system.

C. Junming, J. Yunxia, et al. of the Chinese Academy of Sciences Shanghai Institute of Optics and Mechanics [43] designed and built a polarization-independent broadband reflection grating with a high-refractive-index contrast double-layer isosceles trapezoidal grating ridge and a periodic multilayer-dielectric-film structure in 2017. The high-refractive-index contrast structure comprises several component combinations. This study demonstrated several grating design approaches. Figure 17 shows that the −1st order diffraction efficiencies in the 1020–1100 nm region were 99.57, 99.23, and 99.89%, respectively. The isosceles trapezoid design structure is easier to produce than the rectangular structure, and the dual-layer grating structure with high-refractive-index contrast enables efficient broadband polarization-independent diffraction gratings. The diffraction efficiency in the 1023–1080 nm region surpassed 98%, and Figure 18 shows the as-produced grating topography and reflection diffraction-efficiency spectrum. The broadband polarization-independent multilayer dielectric film grating may be employed as an excellent beam-combining device in a spectral beam-combining system, increasing the power of a system.

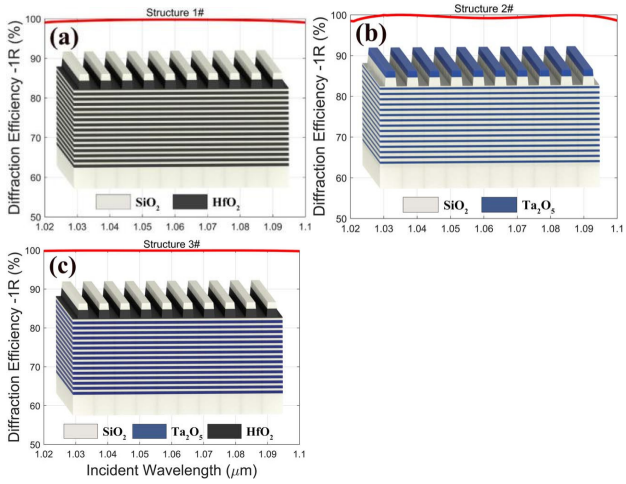

Figure 17. Different grating designs in the 1020–1100 nm band: (**a**) −1st diffraction efficiency = 99.57%, (**b**) −1st diffraction efficiency = 99.23%, and (**c**) −1st diffraction efficiency = 99.89%.

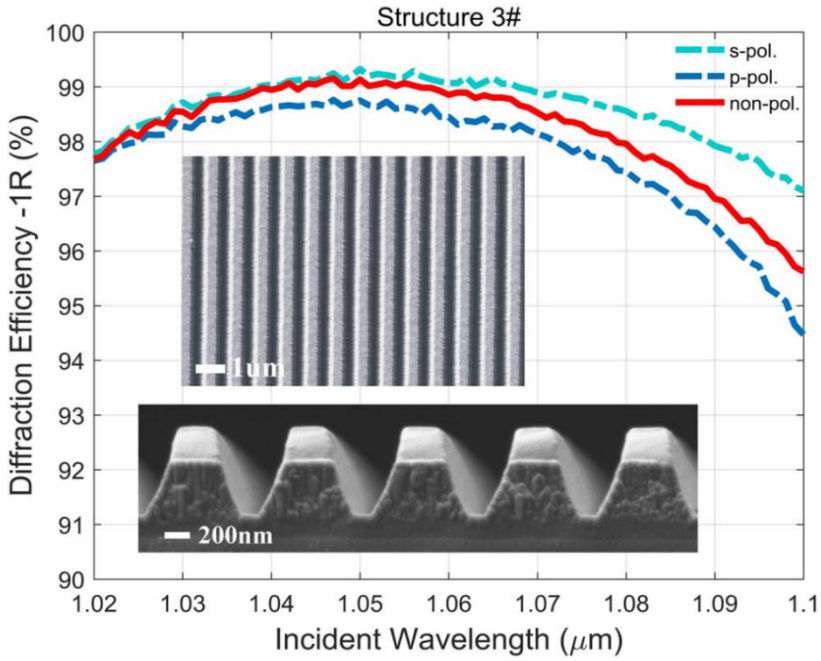

Figure 18. SEM image of a multilayer-dielectric-film reflection grating and a −1 order polarization-independent diffraction-efficiency spectrum.

The same year, L. Linxin, L. Quan, et al. [44] devised and manufactured a revolutionary dual-layer-grating-ridge polarization-independent broadband reflection grating, which was primarily employed in an external-cavity SBC system. The grating structure was mostly made up of a multilayer-dielectric-reflective film and a double-layer-grating ridge structure on the surface. The structure of the multilayer-dielectric-reflective film stack is K9 (optical glass) | $(HL)^{10}H$ | Air. The film was deposited by electron-beam thermal evaporation, where H represents 88.35 nm Ta_2O_5 and L represents 248.60 nm SiO_2; the double-layer grating ridges were 320 nm HfO_2 and 380 nm SiO_2. It was fabricated by full-system exposure and reactive ion-beam etching. The grating period was 1041.67 nm, the duty cycle was 0.73, the Littrow angle was 30.25°, and the bottom angle of the trapezoidal ridge was $\theta_g = 80°$. Figure 19 depicts a cross-sectional SEM image. The grating SiO_2 residual-layer thickness was 300 nm, the −1st order diffraction efficiency in the 1010–1080 nm band region was 95%, and the output power after beam combining was 10.77 kW.

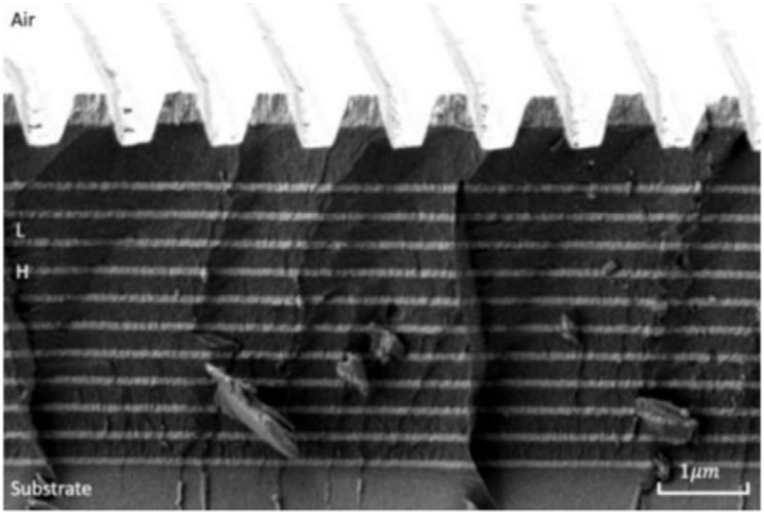

Figure 19. SEM image of a grating cross-section.

C. Hongchao and W. Jun of the Chinese Academy of Sciences Shanghai Institute of Optics and Mechanics devised and built an effective polarization-independent broadband multilayer-dielectric-film reflection grating in 2018 [45]. The top layer grating-groove structure was a combination trapezoid and groove structure that resembles a bullet. The reflection grating's exact technical specifications were as follows: the center wavelength was 1066 nm, the grating period was 900 nm, the first-order diffraction efficiency was 91% in a bandwidth of 50 nm, and the peak diffraction efficiency was 96%. In theoretical design and testing, the following connection exists between diffraction efficiency and wavelength (Figure 20). The multilayer-dielectric-film structure is $(HL)^{14}H$, where H represents HfO_2 with a thickness of 146.57 nm, L represents SiO_2 with a thickness of 199 nm, and the top grating layer is 1338 nm; the designed grating was created using holographic-exposure and inductively-coupled-plasma etching technology. As seen in the SEM image in Figure 21, the as-fabricated grating sample was acquired, and is high efficiency, polarization-independent, and broadband.

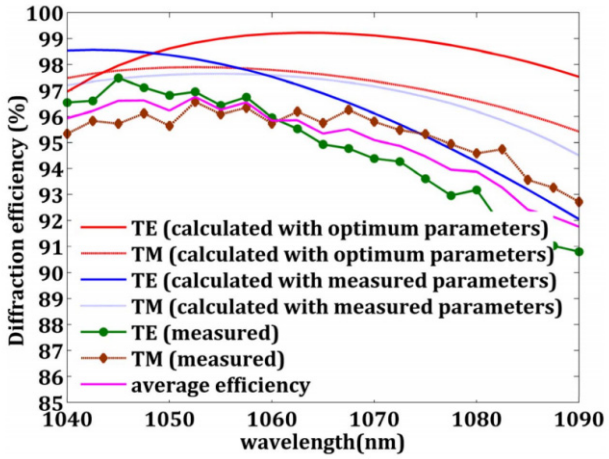

Figure 20. Relationship between the diffraction efficiency and wavelength of the theoretical calculation and the actual measurement.

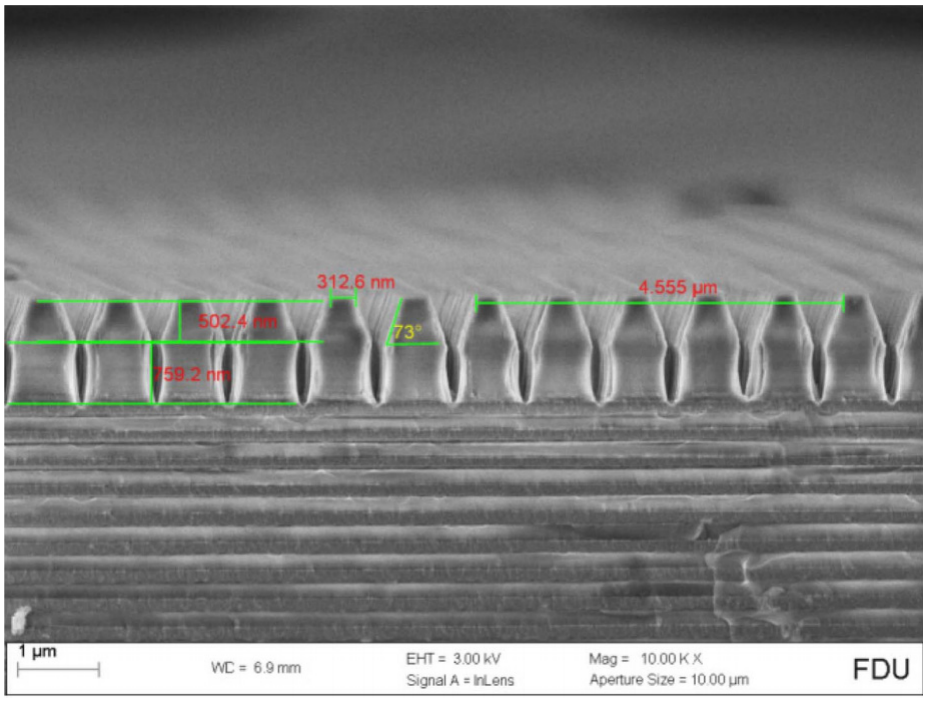

Figure 21. SEM image of the as-prepared grating.

M. Xinyu, L. Chaoming, et al. [46] devised and built a polarization-independent multilayer-dielectric-film reflection grating with a larger linear density for spectral beam combining in 2020. The exact structural characteristics were as follows: quartz substrate, 1300 lines/mm scribe line density, center wavelength 1065 nm, better than 97% diffraction efficiency in the bandwidth of under −1 order Littrow structure, and Sub | $(HL)^{16}$ BGT | C multilayer-dielectric-film structure. H denotes Ta_2O_5 with a thickness of 91 nm, L denotes SiO_2 with a thickness of 284 nm, B denotes Ta_2O_5 with a thickness of 98 nm, G denotes SiO_2 with a thickness of 151 nm, and T denotes Ta_2O_5 with a thickness of 332 nm. The top two layers of the GT structure were etched with grating grooves. The discrepancy between the theoretical and actual test diffraction efficiencies was approximately 2%, which is within a tolerable range, and there were discrepancies between the manufactured and intended grooves, as shown in Figure 22.

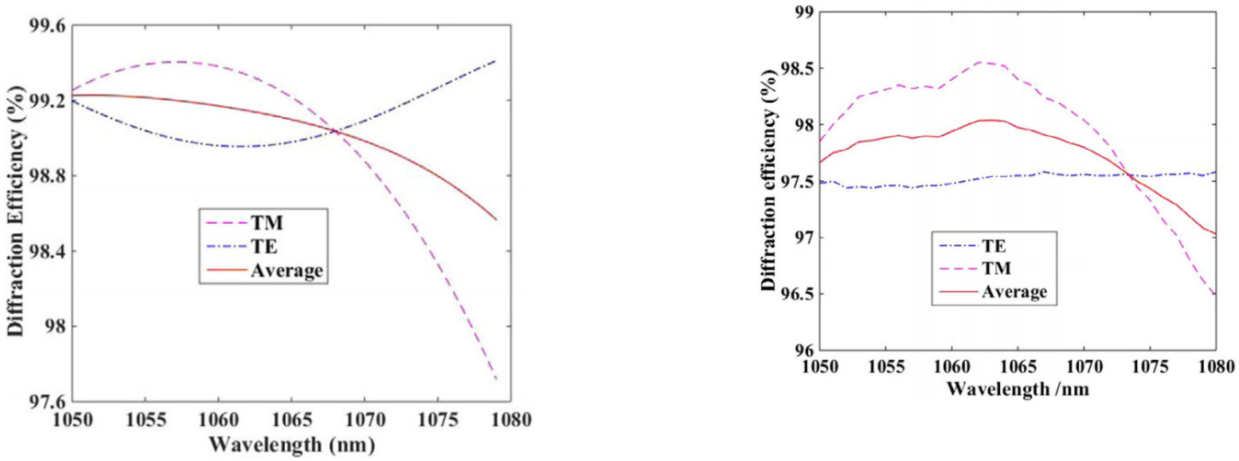

(**a**) (**b**)

Figure 22. (**a**) Theoretical diffraction efficiency and (**b**) actual diffraction efficiency.

Multilayer dielectric reflection gratings continue to play an important role in the development of ultrashort, high-power laser systems. The most appealing characteristics of such gratings are their better diffraction efficiencies and resilience to laser damage compared with those of ordinary metal gratings. A summary of the above analysis is shown in Table 2. Appropriate groove depth and duty cycle index may improve grating diffraction efficiency while minimizing manufacturing complexity, and laser-damage resistance can be considerably increased by combining materials with high damage-resistance thresholds, such as hafnium oxide and silicon dioxide. Furthermore, in the design and production process of the multilayer dielectric film, the anti-laser-damage ability of the film can be effectively improved by optimizing the design structure of the multilayer dielectric film, for instance, with the introduction of buffer layer technology; the performance of components can also be effectively improved by relieving stress through vacuum step annealing. Threshold, high-efficiency, and high-damage reflection gratings are further prospective study issues.

Table 2. Overview of multilayer-dielectric-reflection gratings in recent years.

Years	Units	Structures/Contributions	Performance
1992	LLNL [27]	MDG proposed for the first time	DE > 98%
1993	LLNL [28]	First production	DE > 97% @1053 nm
1995	M. D. Perry, R. D. Boyd, et al. [29]	Line density 1550 gr/mm, multilayer dielectric film $(HL)^S$ H, ZnS/ThF_4	−1st order reflection efficiency over 96%, λ_0 = 1053 nm, TE mode $\theta_{Littrow}$ = 56°

Table 2. *Cont.*

Years	Units	Structures/Contributions	Performance
1997	B. W. Shore, M. D. Perry, et al. [30]	Line density 1480 line/mm, duty cycle 0.3, $(HLL)^n$, HfO_2/SiO_2	−1st order DE = 95%, λ_0 = 1053 nm, TE mode $\theta_{Littrow}$ =51.2°
1999	Karl Hehl, Joerg Bischoff, et al. [31]	Period 380 nm, $(HL)^{10}$ L, Nb_2O_5/SiO_2	−1st DE = 97%, LIDT = 4.4 J/cm^2 @5 ns, $\lambda_{Littrow}$ = 532 nm, TE mode, θ_i = 45°
2005	N. Destouches, AV Tishchenko, et al. [33]	Period 560 nm, multilayer dielectric reflective film Ta_2O_5/SiO_2	−1st DE = 99%, λ_0 = 1064 nm, θ_i = 73°
2007	J. Neauport, E. Lavastre, et al [34]	1780 L/mm, multilayer dielectric film $(HL)^7H$, HfO_2/SiO_2	R = 99.5% @1053 nm; LIDT = 0.67 J/cm^2, θ_i = 70.6°
2014	Martin Rumpel, Michael Moeller, et al. [41]	Line density 1250 line/mm, duty ratio 0.25	−1st DE = 99.35% @1030 nm, DE = 99.7% @1060 nm, θ_i = 44°, LIDT = 2.95 J/cm^2 @12 ns
2016	Yifeng Yang [42]	Line density 960 line/mm,	−1st DE > 95% @1040–1090 nm, θ_i = 30.9°, M^2 = 1.9
2017	Yunxia Jin, Junming Chen, et al. [43]	Sub+ HR+ Double-Layer Isosceles Trapezoidal Grating Ridges	DE > 98% @1023–1080 nm
2018	Hongchao Cao, Jun Wu, et al. [45]	Period 900 nm, $(HL)^{14}H$, HfO^2/SiO_2, top grating layer 1338 nm	λ_0 = 1066 nm, −1st DE = 91% (50 nm), θ_i = 30.9°
2020	Chaoming Li, Xinyu Mao, et al. [46]	1300 gr/mm, Quartz | $(HL)^{16}$ BGT | C, Ta_2O_5/SiO_2	λ_0 =1065 nm, Littrow structure, −1st DE > 97% (30 nm)

2.2.2. Multilayer Dielectric Film Transmission Grating

All-dielectric transmission gratings with high diffraction efficiencies and anti-laser-damage thresholds have garnered a significant amount of attention in recent years and are widely utilized in DWDM, CPA systems, and SBC systems.

C. Enger and S. K. Case [47] created a transmission grating with a grating period of 330 nm, groove depth of 370 nm, and incidence angle of 42° in 1983. The diffraction efficiency of the transmission grating created by holographic exposure was better than 88% at 632.8 nm.

H. T. Nguyen, B. W. Shore, et al. [48] devised and built a high-efficiency fused-silica transmission grating for high-power ultraviolet laser systems in 1997. The grating period was 350 nm, the Littrow blaze angle was 30°, the duty cycle was 0.5, and the groove depth was 600 nm. The theoretical diffraction efficiency of −1 order under TE polarization was 98%. Interference lithography and ion-beam etching were used to create the transmission grating. Except for a 4% shift near the peak, the grating diffraction efficiency was extremely close to the predicted efficiency. The grating diffraction efficiency was 94%. The transmission grating's anti-laser-damage threshold was evaluated using a 3 ns pulse Nd:YAG laser. The grating was positioned at a 30° angle to the TE polarized beam. The anti-laser-damage thresholds were 13.2 J/cm^2 from both the front and rear surfaces. The computed findings matched the experimental readings rather well.

In 2003, T. Clausnitzer, J. Limpert, et al. [49] designed and fabricated a high-efficiency fused-silica transmission grating in the 1064 nm band with a grating period of 800 nm, an incident angle of 41.5° under the Littrow structure, a groove depth of 1540 nm, and a duty cycle of 0.45. The highest diffraction efficiency was 97%. Manufacturing tolerances allowed

trench depths of 1450 to 1650 nm and duty cycles of 0.32 to 0.52. Compared with those of the traditional gold-coated grating, the designed multilayer dielectric grating has a higher diffraction efficiency and anti-laser-damage threshold. The measured anti-laser-damage threshold of the grating under a 170 ns pulse was 2400 J/cm^2. The transmission grating was applied to the ytterbium-doped fiber CPA system to obtain 400 fs pulses with an average power of 76 W.

S. Wang, C. Zhou, et al. devised and built a high-efficiency fused-silica transmission grating in the 1550 nm region in 2006 [50]. No one had considered using a high-efficiency transmission grating of 1550 nm in a dense wavelength-division multiplexing system, according to the report. The grating duty cycle was 0.5, and the grating groove had a rectangular form. Figure 23 depicts the connection between the density of the grating lines, the depth of the grooves, and the diffraction efficiency. It can be seen from the figure that the diffraction efficiency of the grating exceeded 95% when the density of the grating was 650–750 lines/mm and the depth of the grooves was 2500–3000 nm. It is clear from Figure 24 that the sidewall of the grating was steep, the groove depth of the grating was 2500 nm, the linear density of the grating was 674 lines/mm, and the duty cycle was 0.5. The diffraction efficiency of the TM and TE modes in the range of the incident angle range 15–45° was tested experimentally. The highest diffraction efficiency was 87.1% at 31.5°. To manufacture a transmission grating close to the design index, a high-quality fused-silica substrate should be utilized, the grating creation process should be accurately controlled, and an appropriate multilayer dielectric film should be coated on the back of the grating after it has been etched.

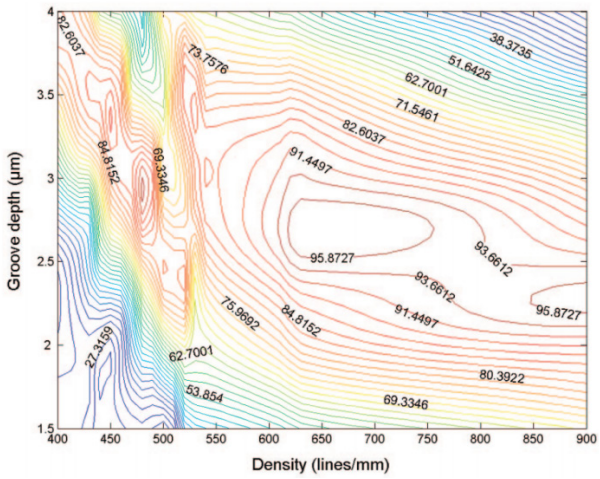

Figure 23. Theoretical efficiency of a fused-silica grating with λ = 1550 nm, m = −1 order, and TE polarization as a function of groove depth and line density for a rectangular profile with a duty cycle of 0.5.

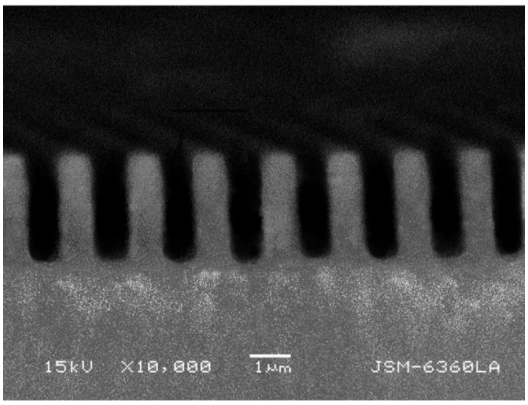

Figure 24. Fabricated fused-silica grating with a density of 674 lines/mm, a groove depth of 2.5 μm, and a duty cycle of 0.5.

In a previous report [51], it was noted that the design of rectangular transmission gratings overlooked the reflection effects of air and the substrates. This explained why the diffraction effectiveness of fabricated gratings of this type was always less than the projected 100%. T. Clausnitzer, T. Kämpfe, et al. [52] proposed a new method in 2008 that uses the buried method to fabricate a multilayer-dielectric-film transmission grating with 100% diffraction efficiency and high dispersion. Furthermore, the damage and pollution of the grating surface structure were effectively reduced. The grating density of the designed buried transmission grating was 1670 lines/mm, and the incident wavelength was 1064 nm. The commercial software Gsolver was used to simulate and analyze the relationship between the duty cycle, groove depth, and grating diffraction efficiency, as shown in Figure 25. When the duty cycle was 0.57 and the groove depth was 1440 nm, the theoretically calculated diffraction efficiency was 99.9%. As shown in Figure 26, the diffraction efficiency was numerically simulated for the corresponding surface-relief grating, and the diffraction efficiency reached a maximum of 93%, which is insufficient for many optical configurations.

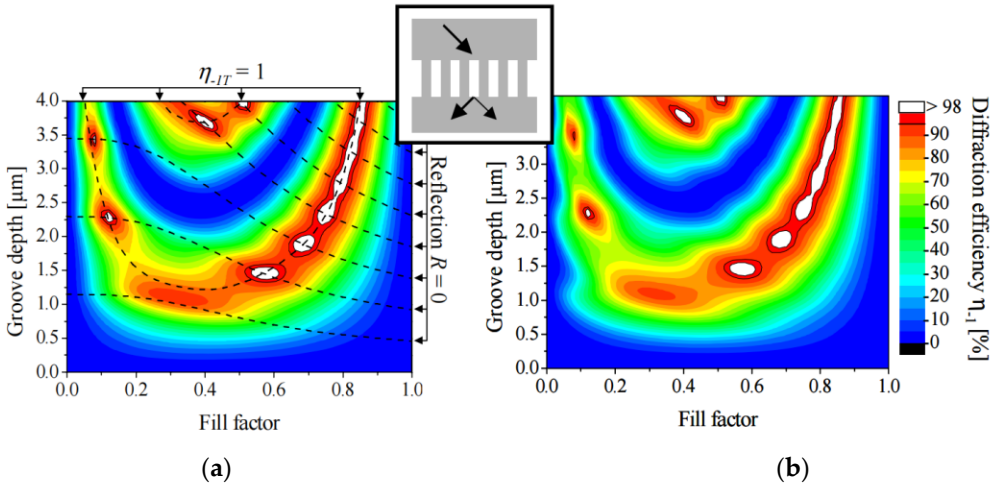

Figure 25. (**a**) Simulation of the diffraction efficiency of a buried grating with a 600 nm period as a function of the profile parameters (wavelength 1064 nm and Littrow configuration). (**b**) Corresponding numerical calculation by rigorous Fourier modal method.

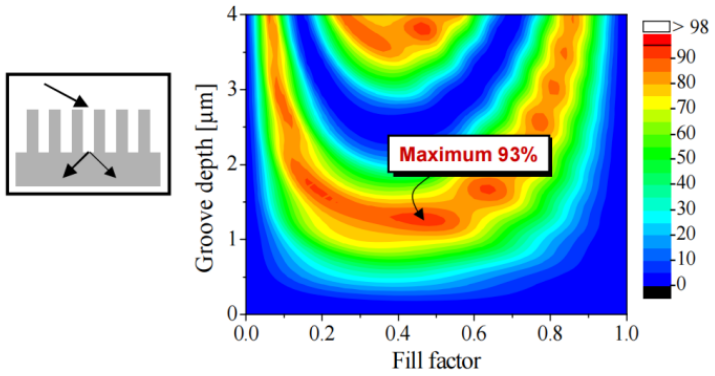

Figure 26. Numerical simulation of the diffraction efficiency of the corresponding surface-relief grating. The maximum diffraction efficiency was 93%.

J. Feng, C. Zhou, et al. [53] suggested a dual-function polarization-selective fused-silica transmission grating with a grating period of 1216 nm and a groove depth of 2314 nm in 2009. FDTD simulations convincingly confirmed the dual function of the transmission grating, with the magnetic field amplitude of the two-port beam splitter exhibiting two-beam interference fringes in the TM mode with a contrast ratio close to 100%. The plot of

the real part of the electric field of the high-efficiency grating in TE mode demonstrates that almost all of the diffracted waves were in the −1 order, as illustrated in Figure 27. The grating may perform the twin functions of a one-to-two beam splitter and a −1 order high-efficiency grating by selecting one of two orthogonal polarization conditions. The transmission grating was created using holographic exposure and inductively coupled plasma; an SEM image is presented in Figure 28. The grating profile was nearly rectangular in form.

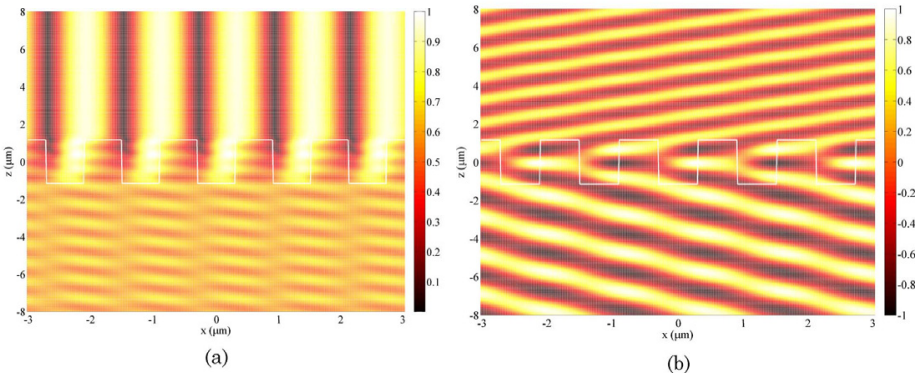

Figure 27. Near-field distribution for a dual-function grating with a period of 1216 nm and a depth of 2314 nm, using the FDTD method at a wavelength of 1550 nm. The incident light was from the bottom, and output waves traveled upward through the grating. (**a**) Amplitude of the output magnetic field for TM polarization, indicating the two-beam interference that was due to the propagation of two equally split beams of the grating. (**b**) Real part of the output electric field for TE polarization, indicating the highly efficient diffraction at the −1st order direction of the grating.

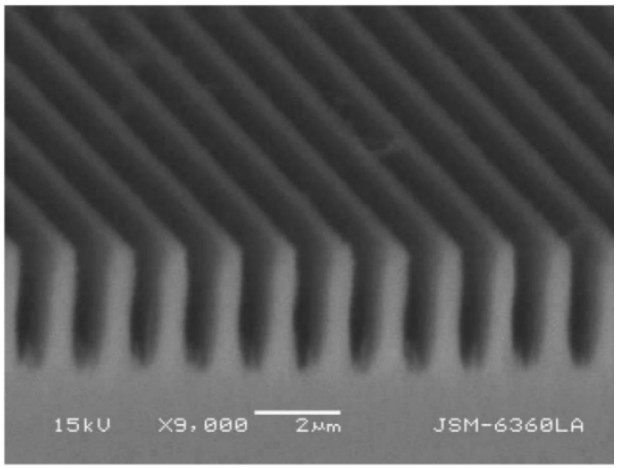

Figure 28. SEM image of the manufactured a dual-function transmission grating.

H. Cao, C. Zhou, et al. [54] undertook related research on near-infrared transmission gratings in 2010, designing and fabricating a −1 order transmission grating for high-power CPA systems. At a wavelength of 800 nm, both TE- and TM-polarized diffraction efficiencies were greater than 97%. Both TE- and TM-polarized waves resulted in diffraction efficiencies greater than 92% within the wavelength range of 750 to 850 nm. Theoretical simulation showed that there was a difference between the grating parameters and diffraction efficiency. The relationship is shown in Figure 29. The incident angle was 32.2°, the duty cycle was 0.67, and the groove depth was 1950 nm. Fused-silica gratings were fabricated by holographic exposure and inductively coupled plasma-etching techniques, and the as-prepared grating morphology is shown in Figure 30. The experimental results were consistent with the theoretical values.

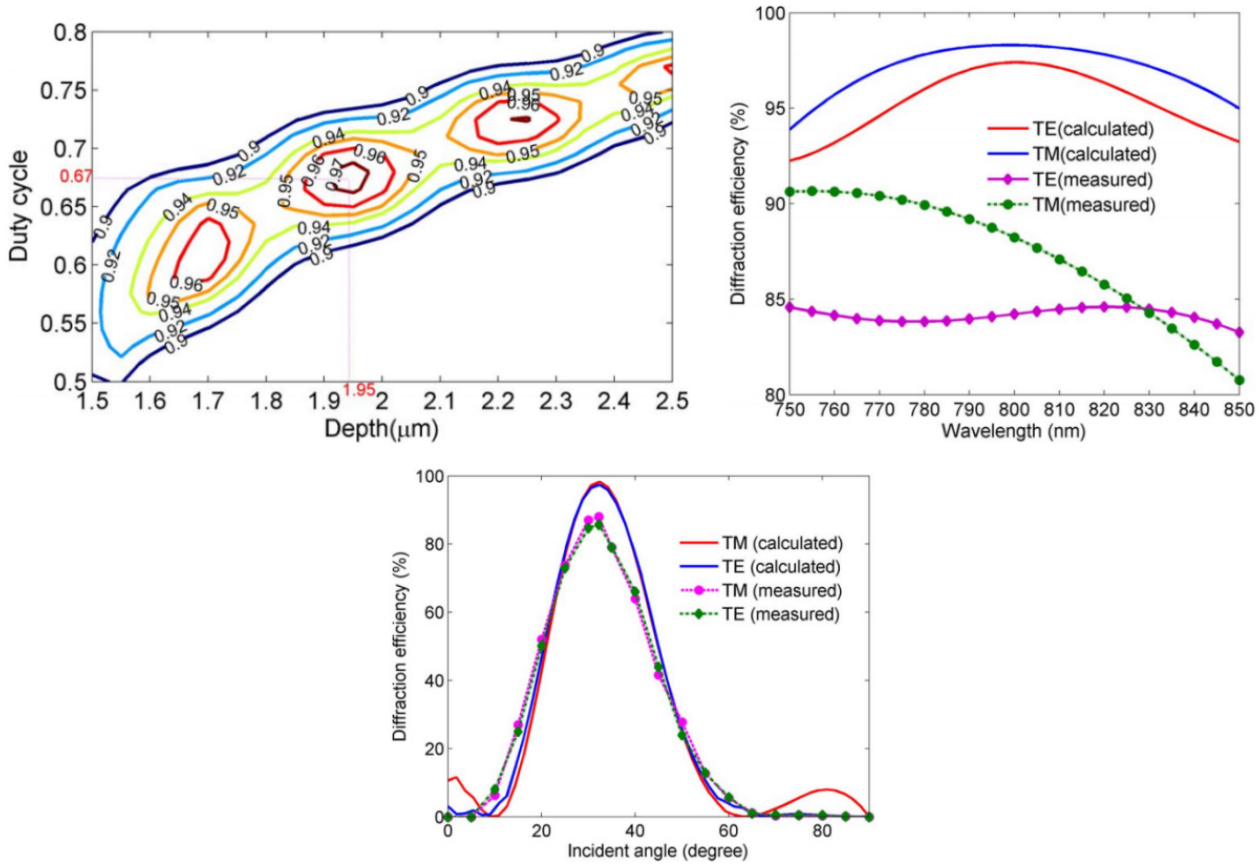

Figure 29. Theoretical and experimental (lines with markers) diffraction efficiencies of the manufactured grating at different incidence angles for TM and TE polarizations.

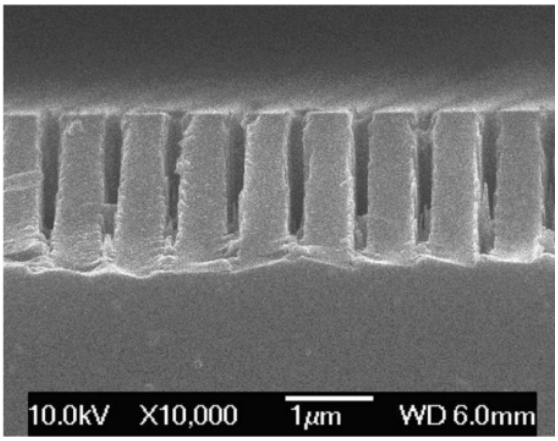

Figure 30. SEM image of the manufactured grating.

In the same year, H. Cao, C. Zhou, et al. [55] designed a high-efficiency triangular-grooved fused-silica transmission grating for the polarization-independent C + L band. After using rigorous coupled-wave analysis (RCWA) optimization to acquire the exact grating parameters, the diffraction efficiency at 101 nm (1500–1601 nm) TE and TM polarizations was better than 90%, while the diffraction efficiencies of both polarizations were greater than 99% at a wavelength of 1550 nm. This is a novel approach to fabricating a transmission grating out of highly dispersive material that can eliminate any reflection loss and achieve 100% diffraction efficiency. Figure 31 depicts the link between grating parameters and diffraction efficiency.

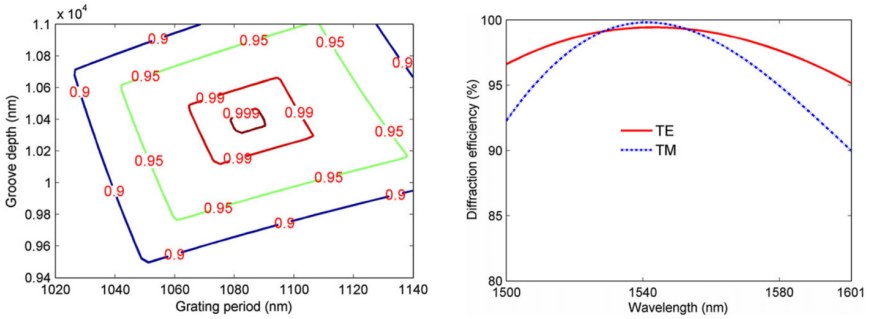

(**a**) (**b**)

Figure 31. (**a**) Contour of the minimum −1st order diffraction efficiencies between TE and TM polarizations versus groove depth and grating period. (**b**) Plot of the −1st order diffraction efficiencies versus incident wavelength, with grating period Λ = 1080 nm, h = 10,300 nm, and θ_i = 45.85° (Littrow angle for 1550 nm incident wavelength).

In 2011, C. Zhou, T. Seki, et al. [56] in Japan developed and manufactured a 170 × 40× 1 mm^3 high-efficiency fused-silica transmission grating with a line density of 1250 lines/mm for terawatt-scale Ti–sapphire lasers. The incidence angle was 30°, and the backside was anti-reflection (AR)-coated. Figure 32 depicts the as-fabricated grating morphology. The diffraction efficiency of the transmission grating in the 750–850 nm band was greater than 90%. The relationship between the duty cycle, groove depth, and diffraction efficiency is shown in Figure 33. Under TE polarization, the incidence angle was 30°, the wavelength band was approximately 800 nm, the duty cycle was 0.49, and the depth was 1380 nm; the diffraction efficiency of the transmission grating reached up to 98%.

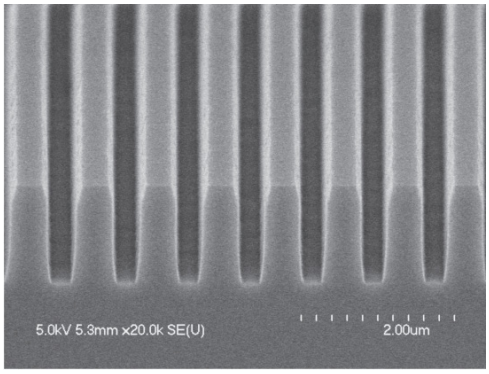

Figure 32. Representative SEM image of the transmission grating.

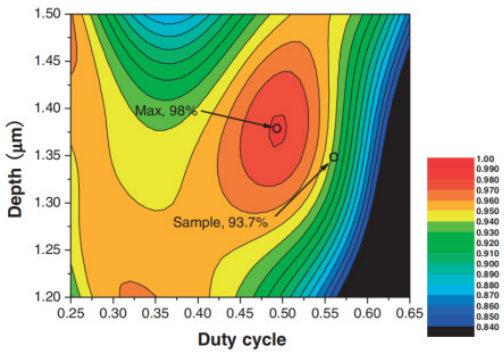

Figure 33. Calculated contour maps of the efficiency at 800 nm with an incidence angle of 30° for TE polarization. The horizontal and vertical axes are the duty cycle and depth of grooves, respectively. The maximum efficiency was 98%, with a duty cycle of 0.49 and depth of 1380 nm.

Expected efficiency was 93.7%, with an actual duty cycle of 0.56 and a depth of 1350 nm.

X. Jing, J. Zhang, et al. [57] created a high-efficiency fused-silica transmission grating with a deeply etched triangular groove shape in 2012. The wavelength at the center was 1064 nm. When the diffraction efficiency of the triangular-groove grating was compared with those of the rectangular grating and the blazed grating, it was determined that the triangular-groove grating was the most efficient diffractive optical element in the −1 order. Transmission gratings designed with fused silica can exhibit significantly improved laser-damage thresholds [41] and have potential applications in high-power laser systems.

Y. Kobayashi, N. Hirayama, et al. [58] devised and manufactured a 180 × 40 mm fused-silica transmission grating with a diffraction efficiency of 96% for an ytterbium fiber laser CPA system in 2013. The transmission grating with the best diffraction efficiency is now used in the high-power Yb fiber system. The grating line density was 1250 lines/mm, the groove depth was 1450 nm, and the duty cycle was 0.45.

The same year, B. Wang, L. Chen, et al. [59] devised and manufactured a broadband deeply etched two-layer transmission grating with minimal polarization dependency to achieve high diffraction efficiency. The first layer was Ta_2O_5 with thickness h_1, the second layer was SiO_2 with thickness h_2, the grating period was 1100 nm, the duty cycle was 0.6, and the incident wavelength was 1550 nm. The modal approach was utilized to evaluate the two-layer grating, and the phase accumulation between the excitation modes of the two layers may be used to show the incident-wave propagation process and explain the high-efficiency grating. The precise depth of the two-layer grating layer may be tuned using RCWA. Figure 34 depicts the connection between the two-layer grating's first order diffraction efficiency and grating depth. When h_1 = 1370 nm and h_2 = 470 nm, the TE and TM polarization efficiencies were 98.23 and 97.44%, respectively. In the depth range of 1300 nm < h_1 < 1390 nm and 360 nm < h_2 < 490 nm, the two polarization efficiencies still reached more than 95%. When the incident wavelength and angle deviated from the central wavelength and Bragg angle within the incident wavelength range of 1514 to 1650 nm or the angle range of 39.071 to 50.641°, the efficiency exceeded 95% under the Littrow installation.

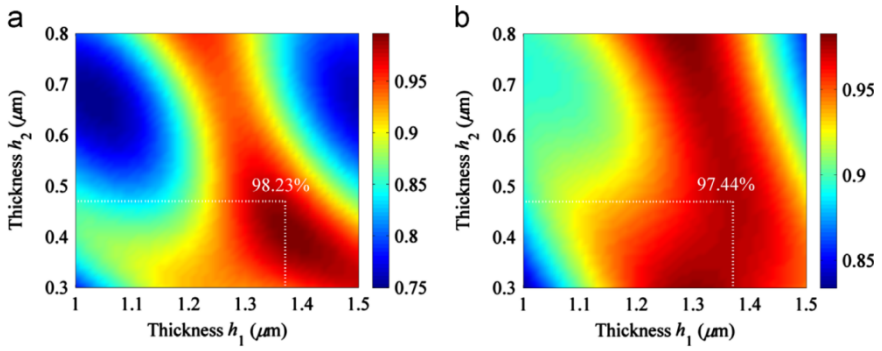

Figure 34. Diffraction efficiency in the –1st order versus grating depths of the two-layer grating: (**a**) TE polarization and (**b**) TM polarization.

Multilayer-dielectric-film gratings are simpler to create than polarization-independent broadband gratings, and they have a higher efficiency than single-layer dielectric film gratings. Z. Yin, J. Yu, et al. [60] created a broadband high-efficiency three-layer all-dielectric rectangular-slot transmission grating with −2 order Bragg incidence in 2020. The three layer structures are composed of Al_2O_3, TiO_2, and SiO_2.

Based on RCWA and a simulated annealing algorithm, the structural parameters of the transmission grating were optimized. The grating period was 1624.6 nm, the duty cycle was 0.4, h_1 was 289.1 nm, h_2 was 904.9 nm, and h_3 was 338.8 nm. At a center wavelength of 1500 nm, with a range of 1454 to 1531 nm and an angle range of 37.32 to 43.3°, the diffraction efficiency of the grating exceeded 95%. The highest efficiency of TE polarization may even reach 99.58% at the second Bragg angle with a wavelength of 1.5 μm. This was the first

time the simplified modal method (SMM) was used to predict the broadband features of multilayer gratings.

Y. Xie, W. Jia, et al. [61] developed a polarization-independent broadband high-efficiency transmission grating in 2021. The grating structure was made up of rectangular grooves with three layers of dielectric films: SiO_2, Si_3N_4, and Al_2O_3. The thicknesses were h_1 = 924.3 nm, h_2 = 571.8 nm, and h_3 = 740.8 nm. The grating period was 1270 nm, and the duty cycle was 0.58. The structure and thicknesses are shown in Figure 35. The incidence angle varied from 32.1 to 42.7° in the 1446–1641 nm range, and the −1st order diffraction efficiency under the Littrow structure was 95%. The grating −1st order diffraction efficiency was 99.1% at the center wavelength of 1550 nm. The 0.0013 dB loss was insignificant.

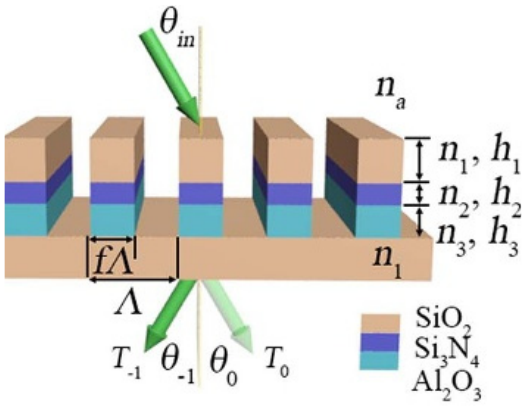

Figure 35. Schematic diagram of the three dielectric layers with a period of 1270 nm and a duty cycle of 0.58 at an incident wavelength of 1550 nm under Littrow incidence.

Summarizing the evolution of transmission gratings in recent years in the Table 3, we conclude that in the visible and near-infrared bands, the majority of transmission grating design structures employ fused silica as the substrate material. Laser-damage thresholds can be greatly improved by using transmission gratings made of fused silica. Depending on the designer's vision of the grating structure, the grating layer material can have either a high refractive index or a low refractive index, commonly combining HfO_2, Ta_2O_5, SiO_2, and other materials. This can not only lessen the difficulties of the manufacturing process but also increase the grating's damage resistance, allowing the transmission grating to be used in a high-power laser system. Furthermore, the anti-laser-damage performance is not only connected to the material but can also be considerably enhanced and improved throughout the manufacturing process. Vacuum step annealing, for example, is used in the process of depositing a multilayer dielectric film to relieve the internal stress of the film layer, enhance the growth structure of the film layer, and increase the element's damage resistance.

Table 3. Overview of multilayer dielectric transmission gratings in recent years.

Years	Units	Structures/Contributions	Performance
1983	R. C. Enger and S. K. Case [47]	Period 330 nm, groove depth 370 nm,	θ_i = 42°, DE > 88% @632.8 nm
1997	H. T. Nguyen, B. W. Shore, et al. [48]	Period 350 nm, duty cycle is 0.5, groove depth 600 nm	$\theta_{Littrow}$ = 30°, TE mode, −1st DE = 98%, LIDT = 13.2 J/cm^2 @3 ns
2003	Tina Clausnitzer, Jens Limpert, et al. [49]	Quartz substrate, period 800 nm, groove depth 1540 nm, duty cycle 0.45	Λ = 1064 nm, $\theta_{Littrow}$ = 41.5° DE_{max} = 97%, LIDT = 2400 J/cm^2 @170 ns

Table 3. *Cont.*

Years	Units	Structures/Contributions	Performance
2006	Shunquan Wang, Changhe Zhou, et al. [50]	Duty cycle 0.5, etched groove depth 2500 nm, line density 674 lines/mm	Λ = 1550 nm, DE > 95%
2008	T. Clausnitzer, T. Kämpfe, et al. [52]	Scribed line density 1670 grooves/mm, duty cycle 0.57, groove depth 1440 nm,	Λ = 1064 nm, DE = 95%
2009	Jijun Feng, Changhe Zhou, et al. [53]	Period 1216 nm, groove depth 2314 nm	Realize the dual function of 1 × 2 beam splitter, −1st order high-efficiency grating
2010	Hongchao Cao, Changhe Zhou, et al. [54,55]	Duty cycle 0.67, groove depth 1950 nm	λ = 800 nm, θ_0 = 41.5°, DE > 92% (750~850 nm)
2011	Chun Zhou, Takashi Seki, et al. [56]	Line density 1250 lines/mm, duty cycle 0.49, groove depth 1380 nm	θ_0 = 30°, TE mode, λ = 800 nm, DE > 90% (750–850 nm)
2012	Xufeng Jing, Junchao Zhang, et al. [57]	Deeply etched triangular groove structure	λ = 1064 nm
2013	Yohei Kobayashi, Nozomi Hirayama, et al. [58]	Line density 1250 line/mm, groove depth 1450 nm, duty cycle 0.45	DE = 96%
2013	Bo Wang, Li Chen, et al. [59]	Period 1100 nm, duty cycle 0.6,	λ = 1550 nm, DE > 95%
2020	Zhengkun Yin, Junjie Yu, et al. [60]	Period 1624.6 nm, duty cycle 0.4	λ = 1550 nm, −2st Bragg DE > 95%
2021	Yongfang Xie, Wei Jia, et al. [61]	Period 1270 nm, duty cycle 0.58	λ = 1550 nm, −1st Littrow DE > 95%, irrelevant loss 0.0013 dB

3. Progress in Grating Fabrication Technology

Grating design and production are very important in semiconductor and spectroscopic applications. Grating morphology is particularly important, hence many researchers have focused on grating fabrication. To date, mechanical scribing has been widely used, and there are also methods for producing target diffraction gratings by duplicating master gratings, such as holographic lithography, electron-beam lithography, nanoimprinting, and others, combined with etching technology (including dry and wet etching) to prepare gratings with various morphologies. In what follows, an overview and discussion of the recent evolution of the grating fabrication technologies mentioned above is presented.

3.1. Mechanical Scribing Technology

Mechanically scribed gratings are amplitude gratings. Mechanical scribing was the first method used for fabricating gratings, and it involves the process of scribing parallel and equal widths on a metal-coated substrate with a scribing machine. The process of equal spacing includes extruding and polishing the material. In the early years, mechanical scribing combined with ion-beam etching was traditionally used to create diffraction grating masters. However, the production of gratings by this method is a lengthy process.

In the 1780s, Rittenhouse made the first grating with dozens of metal wires on a 13 mm wide K9 substrate and performed corresponding diffraction experiments; Thomas Young did not employ gratings to see distinct spectra until the early 19th century. Rutherford then employed a hydraulically powered scribing machine to increase the precision of grating processing and successfully created a grating with 3500 grooves/mm, bringing diffraction grating processing technology to a new level. R. W. Wood employed mechanical scribing technology in the early 20th century to create infrared blazed gratings with a low scribe-line

density and flame effect [62]. D. A. Davies and G. M. Stiff of Australia conducted experimental research on diffraction gratings with scribing densities of 1276 g/mm, 638 g/mm, and 425 g/mm in 1969, and the association between scribed grating grooves and flame angle, as well as grating diffraction effectiveness, was discovered [63].

In 1996, scientists at Bielefeld fabricated a 1200 lines/mm Mo-Si multilayer blazed grating by mechanical scribing. By optimizing the grating groove type, blaze angle and the best matching of Mo-Si bilayer film thickness, the maximum 1st diffraction efficiency was 32% at a wavelength of 13.8 nm and blaze angle of 0.8°. Compared with the 1st diffraction efficiency of a blazed grating with a blaze angle of 1.6°, the mechanical scribing error and reduction of the roughness in the groove were very important for high diffraction efficiency. The efficient scribing of gratings is of great significance [64].

C. Zeiss of Germany simulated and refined the grating-groove geometry of the mechanically scribed grating and employed a scanning probe microscope to monitor the wear of and mechanically characterize the grating groove, resulting in a scribed grating with an 85% blazing efficiency [65]. When processing gratings, modern research units must still rely on the processing experience of equipment operators to some extent. Engineers must install tools in the scribing equipment and adjust scribing settings to ensure that the diffraction gratings generated fulfill the criteria of use. Optimal adjustment increases both the time and cost of processing. The Changchun Institute of Optics and Mechanics suggested a method in 2019 for altering the diamond location in a scriber to achieve nanoscale groove placement. The control precision of the CIOMP-6 scribing machine was further enhanced by enhancing control techniques, such as creating the optical route, and a range of high-quality gratings are manufactured using this scribing mechanism. The first was a high-efficiency grating with groove densities of 500 g/mm, 768 g/mm, and 1520 g/mm, and blaze angles of 10°, 9.7°, and 12.7°, respectively. The experimental diffraction efficiency was close to the theoretical design efficiency; the RMS values at 632.8 nm were 0.079 λ, 0.109 λ, and 0.145 λ, respectively. The second produced was a high-efficiency echelle grating of 64.285 g/mm, the blaze order was −7, and the PV and RMS values at 632.8 nm were 0.093 λ and 0.014 λ, respectively. The maximum ghost and scattered light intensity of the third echelle grating with a line density of 79 g/mm was cut in half, and the as-fabricated diffraction efficiency approached 90% of the theoretical value [66]. Although researchers have conducted corresponding research on scribed gratings in recent years, the scribing technology requires the use of diamond tools to make diffraction gratings; there is a certain error in scribing accuracy, and it is difficult to achieve if the grating period is too large or the groove depth is too deep. There is a certain deviation from the theoretical design, and there are the problems of ghost lines and high stray light, which limit the application of scribing technology to a certain extent.

3.2. Holographic Exposure

With the advent of lasers, holographic lithography has been researched and applied, and grating preparation technology has entered a new stage of development. The principle of holographic lithography is that two coherent plane waves overlap in space to form a standing wave. Then, the periodic interference light-field distribution is recorded with photoresist and other photosensitive materials to realize the fabrication of periodic pattern masks. The graph period expression is:

$$\Lambda = \lambda/(2\sin\theta)$$

where λ is the wavelength of the incident laser and θ is the incidence angle of the corresponding laser beam. Different incidence angles can result in grating structures with different sizes.

Compared with traditional mechanically scribed gratings, diffraction gratings fabricated by holographic lithography have the advantages of no ghost lines, high signal-to-noise ratios, short fabrication periods, low consumption costs, diverse grating grooves, and large area exposures. Holographic lithography can also be combined with the deposition of

multilayer dielectric films to improve diffraction efficiency. In addition, holographic lithography technology combined with ion-beam etching technology can produce blazed gratings with different angles, which significantly improves the diffraction efficiency of the gratings. Therefore, holographic lithography technology has gradually replaced the application of mechanical scribing technology in some fields. In 1990, scientists such as A. Yen and R. A. Ghanbari of the Massachusetts Institute of Technology used achromatic holographic lithography combined with oxygen-plasma-reactive etching technology to fabricate a holographic grating with a period of 100 nm; an anti-reflection coating was used to suppress the standing wave effect before exposure [67]. In 1999, L. A. Wang and C. H. Lin of Taiwan National University first proposed the fabrication of sub-quarter-micron gratings with periods as small as 0.22 μm by combining deep-ultraviolet (DUV) holographic lithography with silanization [68].

In 2000, researchers such as H. J. Jiang and X.-C. Yuan in Singapore proposed a simple UV holographic lithography technology, in which a double-reactive surface-relief grating was fabricated in a single step by holographic lithography on silica–titania glass. Compared with traditional photoresist-based microfabrication techniques, the single-step fabrication process does not require additional exposure and etching steps or expensive etching equipment [69].

In 2003, researchers in the Czech Republic proposed a new doped-layer structure formed by alternating Ag and $As_{30}S_{70}$, and then used holographic lithography (λ = 514 nm) to fabricate a phase grating with a period of 2 μm; Ag can be completely dissolved in the chalcogenide film after exposure, and the refractive index change leads to the achievement of maximum diffraction efficiencies in multilayer and bilayer systems of 3% and 7%, respectively. The multilayer structure greatly increases the sensitivity of the system to incident light. The sensitivity of the system is five times that of the two-layer system [70].

In 2017, L. Qian, K. Wang, et al. [71] fabricated a grating layer with variable line spacing based on the RCWA method and holographic lithography, with a grating duty cycle of 0.5 and a grating-groove depth of 120 nm. The holographic lithography system used a cylindrical lens placed between the collimating mirror and the sample. The laser wavelength was 442 nm, and the holographic grating period changed monotonically on the surface of the device to obtain resonant-wavelength-tunable features. Under TE polarization, the main reflection peak ranged from 762.1 to 908.3 nm, and the grating period increment in the 22 mm range was approximately 108 nm. It was shown that the changing distances between the collimator and the cylindrical lens may modify the tuning range, and it is simple to achieve a greater tuning range, which means the variable-line-spacing grating has promising application possibilities [71].

Tsinghua University, Beijing's X. Mao, C. Li, et al. created a polarization-independent grating in 2020 utilizing computer codes based on precise electromagnetic theory. In addition, holographic exposure paired with ion-beam etching technology was used to create a 1300 lines/mm spectrum beam-combining multilayer dielectric reflection grating. Its center wavelength was 1065 nm, and the diffraction efficiency of the −1st Littrow angle and TE polarization grating in the bandwidth of 30 nm was more than 97% [46].

The holographic lithography method also has its drawbacks. It can only be produced with photoresist. The produced grating has weak durability, and the surface relief structure is prone to impurities, which cannot be cleaned, resulting in a diffraction grating performance that is significantly reduced. In addition, the production of large-sized gratings is limited, and the splicing technology needs to be combined, which also makes for considerable difficulties in the production of large-sized gratings.

3.3. Electron Beam Exposure

At present, lithography technology has undergone several generations of development, and the exposure mode has also changed from the initial-contact type to the projection type, and then to the electronic-scanning type. Exposure patterns are also gradually developing towards smaller line widths and higher precision, and electron-beam lithography

technology has emerged accordingly. Electron-beam lithography is an important patterning method for nanosystems and devices, especially in mask fabrication. Electron-beam lithography is a relatively old patterning method, but it is still the most useful patterning technique in nanofabrication. In the 1980s, more and more nanolithography technologies flourished. Electron-beam lithography offers the unique advantages of high-resolution feature size, high-reliability processing, high-precision alignment, and flexibility for high pattern replication.

In the early 1990s, S. Babin and A. Tomnikov of the Russian Institute of Physics and Technology used the ZBA-20 variable-shape electron-beam lithography system to fabricate an artificial crystal refractive-index grating with a feature size much smaller than the wavelength of the incident light (period 2–3 μm, variable duty cycles, grating area 20 × 20 mm^2, and two-dimensional zero-order grating). Its principle provides an opportunity to generate a medium with a desired refractive-index profile and design an ideal refractive-index distribution by calculating the duty cycle of each period of the optical element, providing a new degree of freedom for the fabrication of optical elements. After photolithography, plasma is used to coat and etch a metal layer, and finally the CO_2 laser beam is focused into a line using the fabricated grating structure [72].

In 2000, H. J. Jiang, X.-C. Yuan, et al. from Nanyang Technological University in Singapore proposed a simple UV holographic interference lithography technique for fabricating surface-relief gratings on hybrid Si–Ti glass with a laser wavelength of 325 nm. The properties of the sol–gel glass, such as refractive index and film thickness, were discussed. The exposure time was 2 min and the exposure dose was 3.5 mW/cm^2. In contrast to traditional photoresist-based microfabrication techniques, this is a single-step fabrication process that does not involve any etching steps [69].

In 2007, Y. Ishii and J. Taniguchi of Japan used the transparency of inorganic resists to solve the problem of exposure blur. By changing the accelerating voltage from 1 to 4 kV at a holographic exposure dose of 250 $\mu C/cm^2$, a blade-shaped mold for binary optics was fabricated. As shown in Figure 36, the design value of the pattern line width was 200 nm. It can be seen from the figure that the width of the line expanded at low voltage [73].

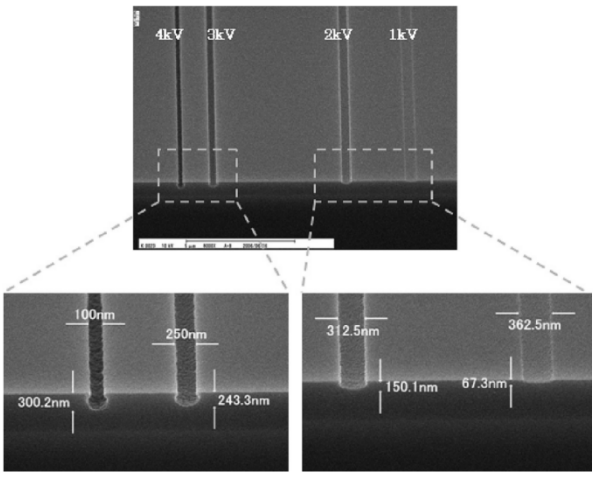

Figure 36. Three-dimensional spin on glass mold diagram.

In 2011, D. L. Voronov et al. of LLNL in Berkeley, California, USA, successfully fabricated a 10,000 lines/mm ultradense sawtooth substrate by electron-beam lithography, then tested it. The fabrication process for the high-quality sawtooth substrates was successfully extended to ultrashort grating periods of 100 nm. The gratings had a near-perfect triangular-groove profile and a very smooth blazed surface [74].

In 2018, J. Turunen and S. Honkanen in Finland proposed a method based on the composition of atomic layers and fabrication of buried-mask gratings. The grating mask was fabricated by electron-beam lithography, and the bottom grating profile was fabricated

in fused silica by reactive-ion etching. Atomic layer deposition was used to prepare an amorphous TiO_2 thin film to bury the SiO_2 grating, which improved the utilization rate of the grating and solved the problem of damage to the grating structure [75].

In electron-beam exposure, the positioning accuracy of the workpiece table and the distortion of the exposure field need to be guaranteed in a very harsh environment. At the same time, the size and direction of the pattern should be designed according to the characteristics of the scanning field of the electron-beam lithography system. In general, the fabrication of diffraction gratings brings great challenges.

3.4. Nanoimprinting

Nanoimprinting is a new micro-nano-pattern processing method. Compared with other preparation methods, nanoimprint lithography (NIL) technology does not rely on optical exposure, is not affected by diffraction, and only relies on the imprint template to deform the upper imprint glue. Nanoimprinting has a series of advantages, such as high resolution, low cost, high yield, and easy operation, which have led to the wider use of nanoimprinting technology, taking the manufacture of gratings to a new height. NIL technology was first proposed by S. Y. Chou [76] of Princeton University in the United States and has been applied in the field of grating fabrication, laying the foundation for the research of many disciplines and practical spectroscopy.

In 2005, S.-W. Ahn et al. of the LG Corporation successfully fabricated an aluminum grating with a line width of 50 nm on a glass substrate using nanoimprinting technology [77]. The grating area reached 5.5 × 5.5 cm, which is the same area as that of a microdisplay panel produced by LG. The grating was used as a metal-grating polarizer, and the polarization extinction ratio exceeded 2000. It had a transmission of 85% for light with a wavelength of 450 nm, and it is currently the best metal-grating polarizer reported. In addition to the expensive imprint templates made by laser interference lithography, the fabrication cost of the monolithic polarizer is low and the efficiency is high. It can already be controlled within the cost range of general parts for consumer electronics. Figure 37 shows a silicon imprint template made by LG and a metal-grating polarizer made with NIL technology.

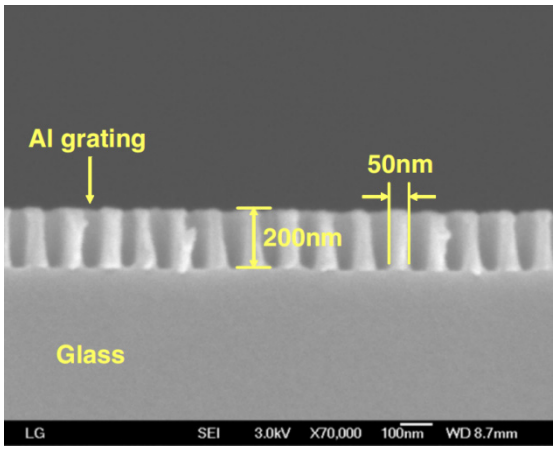

Figure 37. SEM image of an aluminum grating.

In 2011, Z. Jian et al. [78] in Canada prepared molds with rigid UV-curing properties on elastic poly(dimethylsiloxane) (PDMS) scaffolds using three different methods. The first method involves direct imprinting at temperatures above 200 °C. The second method is imprinting onto a curable resist at temperatures below 100 °C, then using reactive ion-beam etching to transfer the pattern into PMGI and write directly by electron-beam lithography. The third method is to use hybrid nanoimprint soft lithography to obtain sub-10 nm feature-size pattern replication, which is short and flexible.

In 2021, F. McGrath, J. Qian, et al. [79] in Ireland proposed a simple method to fabricate silver gratings using silver nanoparticle solutions and nanoimprint lithography

and found that gratings in solutions of silver nanoparticles nanoimprinted directly onto glass substrates have similar properties to those produced by thermally evaporating silver on nanoimprinted PMMA. It was confirmed that this solution-based method does not require special equipment and is more cost-effective than the traditional method of NIL used on PMMA and then thermally evaporated Ag film. In the same year, Professor W. Zhanshan et al. from the Institute of Precision Optical Engineering of Tongji University used a combination of nanoimprint lithography, atomic layer deposition, and reactive ion-beam etching to fabricate a rectangular grating-groove profile with HfO_2 as the material on top of the surface. The PDMS mold was imprinted onto the resist (PMMA), spin-coated on the multilayer dielectric film mirror by UV nanoimprint lithography, and the resist grating structure opposite to the target HfO_2 grating structure was obtained. A rectangular diffraction grating with a diffraction efficiency of 95% (from 714 to 865 nm) and a damage resistance threshold of 0.59 J/cm^2 (40 fs) was fabricated [80].

After the introduction of nanoimprint lithography, certain breakthroughs have been made in grating fabrication, bringing low-cost, high-yield, large-area, and high-density gratings closer and closer to reality.

4. Conclusions

This paper has primarily reviewed the research status of metal-film reflection gratings and multilayer-dielectric-film transmission and the reflection gratings that have been designed and developed. Diffraction grating structural design parameters, fabrication technologies, diffraction efficiency, and anti-laser-damage thresholds have been introduced and analyzed. The analysis shows that metal-film gratings are not able to achieve high diffraction efficiency and anti-laser-damage threshold values due to the inherent absorption characteristics of materials. However, continuous improvements in the theoretical basis and fabrication technologies of diffraction gratings have led to certain breakthroughs. The diffraction efficiencies and anti-laser-damage thresholds of multilayer-dielectric-film gratings have steadily improved, resulting in practical applications. The preparation of diffraction gratings with high damage resistance by optimizing the design of the film structure of the multilayer dielectric film, the groove structure of the diffraction grating, and the near-field distribution of the electromagnetic field is the main focus of future research.

Author Contributions: Writing—original draft preparation, Y.W.; visualization and supervision, X.F., L.Q., Y.N., Y.C. and L.W. All authors have read and agreed to the published version of the manuscript.

Funding: This work is supported by the Ministry of Science and Technology Key R&D Program (2020YFB2205902); the National Natural Science Foundation of China (NSFC) (62090051, 62090052, 62090054, 11874353, 61935009, 61934003, 61904179, 62004194); the Science and Technology Development Project of Jilin Province (20200401069GX, 20200401062GX, 20200501006GX, 20200501007GX, 20200501008GX); the Key R&D Program of Changchun (21ZGG13, 21ZGN23); the Innovation and entrepreneurship Talent Project of Jilin Province (2021Y008); the Key R&D Program of Changchun (21ZGG13, 21ZGN23); the Special Scientific Research Project of Acade-mician Innovation Platform in Hainan Province (YSPTZX202034); and the "Lingyan" Research Program of Zhejiang Province (2022C01108).

Conflicts of Interest: The authors declare no conflict of interest.

References

1. Zhang, J.; Peng, H.; Fu, X.; Liu, Y.; Qin, L.; Miao, G.; Wang, L. CW 50W/M2 = 10.9 diode laser source by spectral beam combining based on a transmission grating. *Opt. Express* **2013**, *21*, 3627–3632. [CrossRef] [PubMed]
2. Vijayakumar, D.; Jensen, O.B.; Ostendorf, R.; Westphalen, T.; Thestrup, B. Spectral beam combining of a 980 nm tapered diode laser bar. *Opt. Express* **2010**, *18*, 893–898. [CrossRef]
3. Daneu, V.; Sanchez, A.; Fan, T.Y.; Choi, H.K.; Turner, G.W.; Cook, C.C. Spectral beam combining of a broad-stripe diode laser array in an external cavity. *Opt. Lett.* **2000**, *25*, 405–407. [CrossRef]
4. Stankeviius, L.; Tamuleviius, T.; Utautas, A.; Juodnas, M.; Tamuleviius, S. Diffraction efficiency optimization of multilayer dielectric mirror-based gratings for 1030 nm femtosecond lasers. *Opt. Laser Technol.* **2020**, *126*, 106071. [CrossRef]

5. Martz, D.H.; Nguyen, H.T.; Patel, D.; Britten, J.A.; Menoni, C.S. Large area high efficiency broad bandwidth 800 nm dielectric gratings for high energy laser pulse compression. *Opt. Express* **2009**, *17*, 23809. [CrossRef] [PubMed]
6. Strickland, D.; Mourou, G. Compression of amplified chirped optical pulses. *Opt. Commun.* **1985**, *56*, 219–221. [CrossRef]
7. Biao, L.; Wen, Z.Y. Design and experiment of spectrometer based on scanning micro-grating integrating with angle sensor. *Infrared Phys. Technol.* **2014**, *62*, 29–33. [CrossRef]
8. Shatokhin, A.N.; Kolesnikov, A.O.; Sasorov, P.V.; Vishnyakov, E.A.; Ragozin, E.N. High-resolution stigmatic spectrograph for a wavelength range of 12.5–30 nm. *Opt. Express* **2018**, *26*, 19009. [CrossRef]
9. Thomae, D.; Hönle, T.; Kraus, M.; Bagusat, V.; Deparnay, A.; Brüning, R.; Brunner, R. Compact echelle spectrometer employing a cross-grating. *Appl. Opt.* **2018**, *57*, 7109–7116. [CrossRef]
10. Yin, K.; Hsiang, E.L.; Zou, J.; Li, Y.; Yang, Z.; Yang, Q.; Lai, P.C.; Lin, C.L.; Wu, S.T. Advanced liquid crystal devices for augmented reality and virtual reality displays: Principles and applications. *Light Sci. Appl.* **2022**, *11*, 161. [CrossRef]
11. Gaylord, T.K.; Moharam, M.G. Thin and thick gratings: Terminology clarification. *Appl. Opt.* **1981**, *20*, 3271–3273. [CrossRef] [PubMed]
12. Molesky, S.; Lin, Z.; Piggott, A.Y.; Jin, W.; Vucković, J.; Rodriguez, A.W. Inverse design in nanophotonics. *Nat. Photonics* **2018**, *12*, 659–670. [CrossRef]
13. Yin, K.; Lee, Y.H.; He, Z.; Wu, S.T. Stretchable, flexible, rollable, and adherable polarization volume grating film. *Opt. Express* **2019**, *27*, 5814–5823. [CrossRef] [PubMed]
14. Yin, K.; He, Z.; Wu, S.T. Reflective Polarization Volume Lens with Small f-Number and Large Diffraction Angle. *Adv. Opt. Mater.* **2020**, *8*, 2000170. [CrossRef]
15. Loewen, E.G. Diffraction gratings: M. C. Hutley. *Precis. Eng.* **1983**. [CrossRef]
16. Yamada, I.; Nishii, J.; Saito, M. Modeling, fabrication, and characterization of tungsten silicide wire-grid polarizer in infrared region. *Appl. Opt.* **2008**, *47*, 4735–4738. [CrossRef]
17. Peng, S.; Quan, L.; Wu, J. Sub-wavelength metal polarization gratings array used in polarization imaging. In Proceedings of the SPIE—The International Society for Optical Engineering, Beijing, China, 17 November 2010; Volume 7848.
18. Jin, Q.; Liu, Q.; Wu, J.; Cheng, Y.; Sheng, Y.; Yu, C.; Chen, L. Design and Fabrication of nanowire-grid polarizer in near-infrared broadband. *Proc. SPIE* **2012**, *8556*, 553–565.
19. Jing, N.; Li, H.Q.; Wen, L. Broadband polarizer or band-pass filter based on a dielectric grating with top and bottom metallic coverings. In Proceedings of the SPIE—The International Society for Optical Engineering, Beijing, China, 13 November 2014; Volume 9277.
20. Xia, Z.; Huang, H.; Kong, F.; Wang, L.; Jin, Y. Varied laser induced damage phenomena of gold coated gratings for pulse compression. *Opt. Lasers Eng.* **2017**, *95*, 42–51. [CrossRef]
21. Xia, Z.; Wu, Y.; Kong, F.; Jin, Y. Using a cover layer to improve the damage resistance of gold-coated gratings induced by a picosecond pulsed laser. *Appl. Surf. Sci.* **2018**, *436*, 362–366. [CrossRef]
22. Zhu, S.Q. *Diffration Grating*; Machine Press: Beijing, China, 1986.
23. Available online: http://www.llnl.gov/nif/lst/diffractive-optics/multilayer.html (accessed on 27 November 2013).
24. Available online: http://www-conf.slac.stanford.edu/lepcf/paper/05_Early.pdf (accessed on 17 April 2000).
25. Kessler, T.J.; Bunkenburg, J.; Huang, H.; Kozlov, A.; Meyerhofer, D.D. Demonstration of coherent addition of multiple gratings for high-energy chirped-pulse-amplified lasers. *Opt. Lett.* **2004**, *29*, 635–637. [CrossRef]
26. Available online: http://www.jobinyvon.fr/frdivisions/Gratings/dielectric_pulse.html (accessed on 23 May 2013).
27. Perry, M.D.; Patterson, F.G.; Weston, J. Spectral shaping in chirped-pulse amplifification. *Opt. Lett.* **1990**, *15*, 381–383. [CrossRef] [PubMed]
28. Perry, M.D. Multilayer dielectric gratings: Increasing the power of light. *Sci. Technol. Rev.* **1995**, 25–33.
29. Perry, M.D.; Shannon, C.; Shults, E.; Boyd, R.D.; Britten, J.A.; Decker, D.; Shore, B.W. High-efficiency multilayer dielectric diffraction gratings. *Opt. Lett.* **1995**, *20*, 940–942. [CrossRef] [PubMed]
30. Shore, B.W.; Perry, M.D.; Britten, J.A.; Boyd, R.D.; Feit, M.D.; Nguyen, H.T.; Chow, R.; Loomis, G.E.; Li, L. Design of high-efficiency dielectric reflection gratings. *J. Opt. Soc. Am. A* **1997**, *14*, 1124–1136. [CrossRef]
31. Hehl, K.; Bischoff, J.; Mohaupt, U.; Palme, M.; Schnabel, B.; Wenke, L.; Bödefeld, R.; Theobald, W.; Welsch, E.; Sauerbrey, R.; et al. High-efficiency dielectric reflection gratings: Design, fabrication, and analysis. *Appl. Opt.* **1999**, *38*, 6257–6271. [CrossRef] [PubMed]
32. Wei, H.; Li, L. All-dielectric reflection gratings: A study of the physical mechanism for achieving high efficiency. *Appl. Opt.* **2003**, *42*, 6255–6260. [CrossRef] [PubMed]
33. Destouches, N.; Tishchenko, A.V.; Pommier, J.C.; Reynaud, S.; Parriaux, O.; Tonchev, S.; Ahmed, M.A. 99% efficiency measured in the -1st order of a resonant grating. *Opt. Express* **2005**, *13*, 3230–3235. [CrossRef] [PubMed]
34. Neauport, J.; Lavastre, E.; Razé, G.; Dupuy, G.; Desserouer, F. Effect of electric field on laser induced damage threshold of multilayer dielectric gratings. *Opt. Express* **2007**, *15*, 12508–12522. [CrossRef] [PubMed]
35. Feit, M.D.; Rubenchik, A.M.; Shore, B.W.; Stuart, B.C.; Perry, M.D. Laser-induced damage in dielectrics with nanosecond to subpicosecond pulses II: Theory. *Proc. SPIE* **1995**, *2428*, 469–478. [CrossRef]
36. Stuart, B.C.; Feit, M.D.; Herman, S.; Rubenchik, A.M.; Shore, B.W.; Perry, M.D. Optical ablation by high-power short-pulse lasers. *J. Opt. Soc. Am. B* **1996**, *13*, 459–468. [CrossRef]

37. Stuart, B.C.; Feit, M.D.; Herman, S.M.; Rubenchik, A.M.; Shore, B.W.; Perry, M.D. Ultrashort-pulse optical damage. In Proceedings of the Laser-induced Damage Threshold in Optical Materials, Boulder, CO, USA, 27 May 1996; Volume 2714, pp. 616–628.
38. Barty, C.; Key, M.; Britten, J.; Beach, R.; Beer, G.; Brown, C.; Bryan, S.; Caird, J.; Carlson, T.; Crane, J.; et al. An overview of LLNL high-energy short-pulse technology for advanced radiography of laser fusion experiments. *Nucl. Fusion* **2004**, *44*, S266–S275. [CrossRef]
39. Keck, J.; Oliver, J.B.; Kessler, T.J.; Huang, H.; Barone, J.; Hettrick, J.; Rigatti, A.L.; Hoover, T.; Marshall, K.L.; Schmid, A.W.; et al. Manufacture and development of multilayer diffraction gratings. In Proceedings of the Laser-induced Damage Threshold in Optical Materials, Boulder, CO, USA, 7 February 2006.
40. Wirth, C.; Schmidt, O.; Tsybin, I.; Schreiber, T.; Eberhardt, R.; Limpert, J.; Tünnermann, A.; Ludewigt, K.; Gowin, M.; Have, E.T.; et al. High average power spectral beam combining of four fiber amplifiers to 8.2 kW. *Opt. Lett.* **2011**, *36*, 3118–3120. [CrossRef]
41. Rumpel, M.; Moeller, M.; Moormann, C.; Graf, T.; Ahmed, M.A. Broadband pulse compression gratings with measured 99.7% diffraction efficiency. *Opt. Lett.* **2014**, *39*, 323–326. [CrossRef] [PubMed]
42. Zheng, Y.; Yang, Y.; Wang, J.; Hu, M.; Liu, G.; Zhao, X.; Chen, X.; Liu, K.; Zhao, C.; He, B.; et al. 108 kW spectral beam combination of eight all-fiber superfluorescent sources and their dispersion compensation. *Opt. Express* **2016**, *24*, 12063–12071. [CrossRef]
43. Chen, J.; Zhang, Y.; Wang, Y.; Kong, F.; Huang, H.; Wang, Y.; Jin, Y.; Chen, P.; Xu, J.; Shao, J. Polarization-independent broadband beam combining grating with over 98% measured diffraction efficiency from 1023 to 1080 nm. *Opt. Lett.* **2017**, *42*, 4016–4019. [CrossRef] [PubMed]
44. Li, L.; Liu, Q.; Chen, J.; Wang, L.; Jin, Y.; Yang, Y.; Shao, J. Polarization-independent broadband dielectric bilayer gratings for spectral beam combining system. *Opt. Commun.* **2017**, *385*, 97–103. [CrossRef]
45. Cao, H.; Wu, J.; Yu, J.; Ma, J. High-efficiency polarization-independent wideband multilayer dielectric reflective bullet-alike cross-section fused-silica beam combining grating. *Appl. Opt.* **2018**, *57*, 900–904. [CrossRef] [PubMed]
46. Mao, X.; Li, C.; Qiu, K.; Zeng, L.; Li, L.; Chen, X.; Wu, J.; Liu, Z.; Fu, S.; Hong, Y. Design and fabrication of 1300-line/mm polarization-independent reflection gratings for spectral beam combining. *Opt. Commun.* **2020**, *458*, 124883. [CrossRef]
47. Enger, R.C.; Case, S.K. High-frequency holographic transmission gratings in photoresist. *J. Opt. Soc. Am.* **1983**, *73*, 1113–1118. [CrossRef]
48. Nguyen, H.T.; Shore, B.W.; Bryan, S.J.; Britten, J.A.; Boyd, R.D.; Perry, M.D. Perry. High-efficiency fused-silica transmission gratings. *Opt. Lett.* **1997**, *22*, 142–144. [CrossRef]
49. Clausnitzer, T.; Limpert, J.; Zöllner, K.; Zellmer, H.; Fuchs, H.J.; Kley, E.B.; Tünnermann, A.; Jupé, M.; Ristau, D. Highly efficient transmission gratings in fused silica for chirped-pulse amplification systems. *Appl. Opt.* **2003**, *42*, 6934–6938. [CrossRef] [PubMed]
50. Wang, S.; Zhou, C.; Zhang, Y.; Ru, H. Deep-etched high-density fused-silica transmission gratings with high efficiency at a wavelength of 1550 nm. *Appl. Opt.* **2006**, *45*, 2567–2571. [CrossRef] [PubMed]
51. Clausnitzer, T.; Kämpfe, T.; Kley, E.-B.; Tünnermann, A.; Peschel, U.; Tishchenko, A.V.; Parriaux, O. An intelligible explanation of highly-efficient diffraction in deep dielectric rectangular transmission gratings. *Opt. Express* **2005**, *13*, 10448–10456. [CrossRef] [PubMed]
52. Clausnitzer, T.; Kämpfe, T.; Kley, E.B.; Tünnermann, A.; Tishchenko, A.V.; Parriaux, O. Highly-dispersive dielectric transmission gratings with 100% diffraction efficiency. *Opt. Express* **2008**, *16*, 5577–5584. [CrossRef] [PubMed]
53. Feng, J.; Zhou, C.; Zheng, J.; Cao, H.; Lv, P. Dual-function beam splitter of a subwavelength fused-silica grating. *Appl. Opt.* **2009**, *48*, 2697–2701. [CrossRef] [PubMed]
54. Cao, H.; Zhou, C.; Feng, J.; Lu, P.; Ma, J. Design and fabrication of a polarization-independent wideband transmission fused-silica grating. *Appl. Opt.* **2010**, *49*, 4108. [CrossRef]
55. Cao, H.; Zhou, C.; Feng, J.; Lv, P.; Ma, J. Polarization-independent triangular-groove fused-silica gratings with high efficiency at a wavelength of 1550 nm. *Opt. Commun.* **2010**, *283*, 4271–4273. [CrossRef]
56. Zhou, C.; Seki, T.; Sukegawa, T.; Kanai, T.; Itatani, J.; Kobayashi, Y.; Watanabe, S. Large-Scale, High-Efficiency Transmission Grating for Terawatt-Class Ti: Sapphire Lasers at 1 kHz. *Appl. Phys. Express* **2011**, *4*, 72701. [CrossRef]
57. Jing, X.; Zhang, J.; Jin, S.; Liang, P.; Tian, Y. Design of highly efficient transmission gratings with deep etched triangular grooves. *Appl. Opt.* **2012**, *51*, 7920–7933. [CrossRef]
58. Kobayashi, Y.; Hirayama, N.; Ozawa, A.; Sukegawa, T.; Seki, T.; Kuramoto, Y.; Watanabe, S. 10-MHz, Yb-fiber chirped-pulse amplifier system with large-scale transmission gratings. *Opt. Express* **2013**, *21*, 12865–12873. [CrossRef]
59. Wang, B.; Chen, L.; Lei, L.; Zhou, J. Modal analysis and numerical design of wideband two-layer grating with low polarization dependence. *Opt. Commun.* **2013**, *306*, 74–77. [CrossRef]
60. Yin, Z.; Yu, J.; Lu, Y.; Zhou, C. Broadband High-Efficiency Gratings Operating at the 2nd Order Designed by Simplified Modal Method. *IEEE Photon. Technol. Lett.* **2020**, *32*, 309–312. [CrossRef]
61. Xie, Y.; Jia, W.; Sun, P.; Xiang, C.; Jin, G.; Liu, W.; Zhou, B.; Zhou, C. Ultra-broadband polarization-independent high-efficiency transmission grating based on three-layer dielectric rectangle groove. *J. Opt.* **2021**, *23*, 075606. [CrossRef]
62. Wood, R.W. LXXXV. The echelette grating for the infra-red. *J. Frankl. Inst.* **1910**, *20*, 770–778. [CrossRef]
63. Mcneill, J.J. Diffraction Grating Ruling in Australia. *Appl. Opt.* **1969**, *8*, 1379. [CrossRef]
64. Kleineberg, U.; Stock, H.J.; Kloidt, A.; Osterried, K.; Menke, D.; Schmiedeskamp, B.; Heinzmann, U.; Fuchs, D.; Miiller, P.; Scholze, F.; et al. Mo/Si multilayer coated laminar phase and ruled blaze gratings for the soft X-ray region. *J. Electron Spectrosc. Relat. Phenom.* **1996**, *80*, 389–392. [CrossRef]

65. Zeiss, C. Custom Designed Gratings [DB/OL]. Diffraction Grating Technical Information. 2004. Available online: http://www.zeiss.de/C12567B00035551E/EmbedTitelIntern/Gratings/$File/Grating_2004 (accessed on 15 June 2002).
66. Mi, X.; Zhang, S.; Qi, X.; Yu, H.; Yu, H.; Tang, Y. Ruling engine using adjustable diamond and interferometric control for high-quality gratings and large echelles. *Opt. Express* **2019**, *27*, 19448. [CrossRef]
67. Yen, A.; Ghanbari, R.A.; Anderson, E.H.; Smith, H.I. Fabrication of 100nm-period gratings using achromatic holographic lithography. *Microelectron. Eng.* **1990**, *11*, 201–205. [CrossRef]
68. Wang, L.A.; Lin, C.H.; Chen, J.H. Fabrication of sub-quarter-micron grating patterns by employing DUV holographic lithography. *Microelectron. Eng.* **1999**, *46*, 173–177. [CrossRef]
69. Jiang, H.J.; Yuan, X.-C.; Zhou, Y.; Chan, Y.C.; Lam, Y.L. Single-step fabrication of diraction gratings on hybrid sol ± gel glass using holographic interference lithography. *Opt. Commun.* **2000**, *185*, 19–24. [CrossRef]
70. Waagner, T.; Schroeter, S.; Glaser, T.; Vlccek, M. Holographic grating preparation in Ag/As30S70 multilayer and bilayer structures. *J. Non-Cryst. Solids* **2003**, *326*, 500–504. [CrossRef]
71. Qian, L.; Wang, K.; Han, C. Tunable Filter With Varied-Line-Spacing Grating Fabricated Using Holographic Recording. *IEEE Photonics Technol. Lett.* **2017**, *29*, 925–928. [CrossRef]
72. Babin, S.; Tomnikov, A. Artificial refractive index gratings manufacturing using electron beam lithography—ScienceDirect. *Microelectron. Eng.* **1995**, *27*, 167–170. [CrossRef]
73. Ishii, Y.; Taniguchi, J. Fabrication of three-dimensional nanoimprint mold using inorganic resist in low accelerating voltage electron beam lithography. *Microelectron. Eng.* **2007**, *84*, 912–915. [CrossRef]
74. Voronov, D.L.; Anderson, E.H.; Cambie, R.; Dhuey, S.; Padmore, H.A. Fabrication and characterization of ultra-high resolution multilayer-coated blazed gratings. *Nucl. Inst. Methods Phys. Res. A* **2011**, *649*, 156–159. [CrossRef]
75. Ali, R.; Saleem, M.R.; Roussey, M.; Turunen, J.; Honkanen, S. Fabrication of buried nanostructures by atomic layer deposition. *Sci. Rep.* **2018**, *8*, 15098. [CrossRef]
76. Chou, S.Y.; Krauss, P.R.; Renstrom, P.J. Imprint of sub-25 nm vias and trenches in polymers. *Appl. Phys. Lett.* **1995**, *67*, 3114–3116. [CrossRef]
77. Ahn, S.W.; Lee, K.D.; Kim, J.S.; Kim, S.H.; Park, J.D.; Lee, S.H.; Yoon, P.W. Fabrication of a 50 nm half-pitch wire grid polarizer using nanoimprint lithography. *Nanotechnology* **2005**, *16*, 1874. [CrossRef]
78. Zhang, J.; Cui, B.; Ge, H. Fabrication of flexible mold for hybrid nanoimprint-soft lithography. *Microelectron. Eng.* **2011**, *88*, 2192–2195. [CrossRef]
79. McGrath, F.; Qian, J.; Gwynne, K.; Kumah, C.; Daly, D.; Hrelescu, C.; Zhang, X.; O'Carroll, D.M.; Bradley, A.L. Structural, optical, and electrical properties of silver gratings prepared by nanoimprint lithography of nanoparticle ink. *Appl. Surf. Sci.* **2020**, *537*, 147892. [CrossRef]
80. Xie, L.; Zhang, J.; Zhang; Z.; Ma, B.; Cheng, X. Rectangular multilayer dielectric gratings with broadband high diffraction efficiency and enhanced laser damage resistance. *Opt. Express* **2021**, *29*, 2669–2678. [CrossRef] [PubMed]